EUROPEAN ORGANIZATION FOR NUCLEAR RESEARCH (CERN)

CERN-EP-2024-313
2025/10/16

CMS-HIG-22-004

Search for a heavy pseudoscalar Higgs boson decaying to a 125 GeV Higgs boson and a Z boson in final states with two tau and two light leptons in proton-proton collisions at $\sqrt{s} = 13$ TeV

The CMS Collaboration*

arXiv:2501.14825v2 [hep-ex] 15 Oct 2025

Abstract

A search for a heavy pseudoscalar Higgs boson, A, decaying to a 125 GeV Higgs boson h and a Z boson is presented. The h boson is identified via its decay to a pair of tau leptons, while the Z boson is identified via its decay to a pair of electrons or muons. The search targets the production of the A boson via the gluon-gluon fusion process, $gg \to A$, and in association with bottom quarks, $b\bar{b}A$. The analysis uses a data sample corresponding to an integrated luminosity of 138 fb^{-1} collected with the CMS detector at the CERN LHC in proton-proton collisions at a centre-of-mass energy of $\sqrt{s} = 13$ TeV. Constraints are set on the product of the cross sections of the A production mechanisms and the $A \to Zh$ decay branching fraction. The observed (expected) upper limit at 95% confidence level ranges from 0.049 (0.060) pb to 1.02 (0.79) pb for the $gg \to A$ process and from 0.053 (0.059) pb to 0.79 (0.61) pb for the $b\bar{b}A$ process in the probed range of the A boson mass, m_A, from 225 GeV to 1 TeV. The results of the search are used to constrain parameters within the $M^{125}_{h,EFT}$ benchmark scenario of the minimal supersymmetric extension of the standard model. Values of $\tan\beta$ below 2.2 are excluded in this scenario at 95% confidence level for all m_A values in the range from 225 to 350 GeV.

Published in the Journal of High Energy Physics as doi:10.1007/JHEP10(2025)074.

© 2025 CERN for the benefit of the CMS Collaboration. CC-BY-4.0 license

*See Appendix A for the list of collaboration members

1 Introduction

The 2012 observation of a Higgs-like boson with a mass of approximately 125 GeV at the CERN LHC [1–3] completed the set of particles predicted by the standard model (SM). In the years since, LHC collaborations have measured the properties of this Higgs boson across various production modes and decay channels, including refined measurements of its mass, coupling strengths to fermions and gauge bosons, and spin-parity quantum numbers [4, 5]. To date, these refined measurements of the observed boson are compatible with SM expectations. In the SM, the Higgs field is introduced as a complex doublet in the electroweak sector, and the Higgs boson emerges as a massive scalar state with couplings to the massive fermions and gauge bosons from the spontaneous breaking of the electroweak gauge symmetry. These couplings are found to be in good agreement, within the currently attained experimental precision of 5–20% [6–9], with the expectation for a SM Higgs boson with mass 125.38 ± 0.14 GeV [10]. The SM still leaves several fundamental questions open, including the presence of dark matter and the observed baryon asymmetry in our universe. Beyond-the-SM (BSM) scenarios seek to extend our understanding to explain such phenomena, for example, by adding structure to its Higgs sector. Two Higgs Doublet Models (2HDMs) are BSM theories introducing a second Higgs doublet, which, following electroweak symmetry breaking, yields five mass eigenstates [11, 12]. Two are charged ($\mathrm{H}^{\pm}$), two are neutral scalars (h, H), and one is a massive pseudoscalar boson A, the subject of this search. Given current experimental constraints, most of the 2HDMs associate the lighter scalar boson h with the observed 125 GeV Higgs boson and we follow this convention throughout the paper. The 2HDMs are motivated because they contain, or allow, for additional sources of CP violation that could explain the observed baryon asymmetry in our universe [13]. The presence of two Higgs doublets is also a requirement in the minimal supersymmetric extension of the SM (MSSM) [14, 15], which offers a dark matter candidate, protects the Higgs boson mass from receiving large radiative corrections, and provides conditions for the unification of gauge interactions at the 10^{16} GeV scale [16].

The MSSM Higgs sector is a Type-II 2HDM, which at tree-level is charaterized by two parameters, usually taken to be $\tan\beta = v_2/v_1$, the ratio of the vacuum expectation values of the two Higgs doublets, and m_{A}, the mass of the A boson. The MSSM Higgs boson masses receive large contributions from radiative loop corrections related to the supersymmetric (SUSY) partners of the SM particles. In many MSSM scenarios, the mass scale of these supersymmetric partners, M_{SUSY}, is assumed to be $\mathcal{O}(1\,\mathrm{TeV})$. With this assumption, the predicted value for m_{h} falls below 125 GeV at $\tan\beta \lesssim 5-7$. Thus, higher scales for M_{SUSY} are required to support the mass of the observed Higgs boson, $m_{\mathrm{h}} \approx 125$ GeV, in the whole parameter space, including values of $\tan\beta$ as low as $\approx$1. This paper addresses a specific MSSM benchmark scenario, called $\mathrm{M}^{125}_{\mathrm{h,EFT}}$ [17]. This scenario uses an effective field theory (EFT) approach, where the growing logarithmic corrections associated with the large values of M_{SUSY} are resummed, and M_{SUSY} can reach 10^{16} GeV and is adjusted to values that are compatible with $m_{\mathrm{h}} \approx 125$ GeV at each point in the m_{A}-$\tan\beta$ parameter space individually. The adjusted value of M_{SUSY} varies in the range from 10^4 GeV for $\tan\beta \sim 10$ to 10^8 GeV at $\tan\beta \sim 1$.

This paper reports a search for a pseudoscalar A boson decaying to a 125 GeV Higgs boson h and a Z boson in proton-proton (pp) collisions at $\sqrt{s} = 13$ TeV. The search uses data collected at the LHC in the period from the year 2016 to 2018, by the CMS experiment, corresponding to an integrated luminosity of 138 fb^{-1}. The analysis targets A boson production via both gluon-gluon fusion, $\mathrm{gg} \to \mathrm{A}$, and in association with b quarks, $\mathrm{b\bar{b}A}$. The Feynman diagrams for both production processes are shown in Fig. 1. Signal mass hypotheses are tested in the range from 225 GeV, near the kinematic threshold for decays to Zh, up to 1 TeV. The analysis strategy is optimized for a resolved topology and relies on conventional techniques to identify isolated

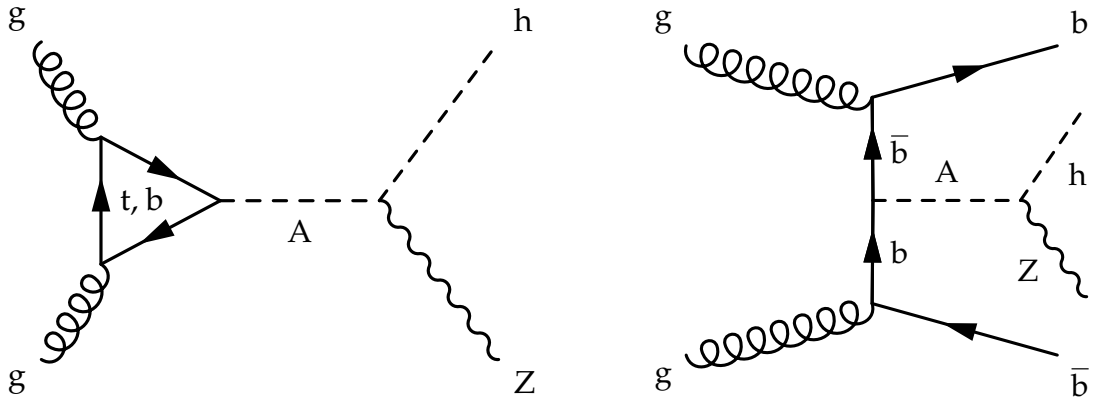


Figure 1: Feynman diagrams representing the production of the pseudoscalar A boson via gluon-gluon m_{A}-tan β fusion (left) and associated production with a bottom quark-antiquark pair (right). In each case, the A boson decays to an SM-like h boson and a Z boson.

leptons. This strategy sustains high sensitivity to the signal for m_{A} up to 1 TeV. At higher A masses, the Z and h bosons are produced with large Lorentz boost, causing the decay products of each boson to be collimated and thus overlapping. As a consequence, the sensitivity of the analysis, targeting resolved topology, rapidly degrades at $m_{\mathrm{A}} > 1$ TeV. It should also be emphasized that most BSM scenarios predict rapidly decreasing branching fractions of bosonic decays of the A boson with increasing m_{A}.

Previous searches by the ATLAS and CMS Collaborations for $\mathrm{A} \to \mathrm{Zh}$ targeted final states with two light leptons from the Z boson decay plus two tau leptons from the h boson decay in pp collision dataset at $\sqrt{s} = 8$ TeV [18, 19] and $\sqrt{s} = 13$ TeV [20]. The ATLAS and CMS Collaborations have also used pp collisions at $\sqrt{s} = 13$ TeV to search for the CP-odd A boson decaying to the same intermediate Zh state, but with the Higgs boson h decaying to a pair of bottom quarks [21–23]. These analyses set model-independent and model-dependent limits in the context of 2HDMs, including supersymmetric models.

In this analysis, the h boson is identified by its decay to a pair of tau leptons. Three possible $\tau\tau$ decay channels are considered: $\mathrm{e}\tau_{\mathrm{h}}$, $\mu\tau_{\mathrm{h}}$, and $\tau_{\mathrm{h}}\tau_{\mathrm{h}}$, where τ_{h} denotes hadronic τ lepton decays. Throughout the paper, neutrinos are omitted from the notation of the final states. These three decay channels are combined with Z boson decays into two light leptons, $\mathrm{Z} \to \ell^+\ell^-$ ($\ell = \mathrm{e}, \mu$), resulting in six distinct final states of the A boson decay. To account for the missing transverse momentum that results from the neutrinos in the final states, we use a modified version of the SVFit algorithm [24], FastMTT [25], to reconstruct the four-vector of h, while constraining its mass to 125 GeV. The signal is extracted from the distributions of the reconstructed four-lepton mass obtained in these individual search channels. Furthermore, to increase the sensitivity to different production modes of the A boson, events are split into two categories depending on the presence of a b quark in the event.

Relative to the CMS search performed using the 2016 data [20], this analysis benefits from the increased integrated luminosity and novel machine learning based identification of hadronic decays of τ leptons [26] and of jets originating from bottom quarks [27]. It also includes the production of an A boson in association with b quarks, a process not considered previously, and extends the range of probed masses of the pseudoscalar boson up to 1 TeV. This analysis provides complementary results to the recent ATLAS search in the $(\mathrm{Z} \to \nu\overline{\nu}/\ell\ell)(\mathrm{h} \to \mathrm{b\overline{b}})$ channels performed on 139 fb^{-1} of data collected at the same centre-of-mass energy [23].

A complete set of tabulated results of the current analysis for all tested mass hypotheses is available in the HEPData record [28].

2 The CMS detector

The central feature of the CMS apparatus is a superconducting solenoid of 6 m internal diameter, providing a magnetic field of 3.8 T. Within the solenoid volume are a silicon pixel and strip tracker, a lead tungstate crystal electromagnetic calorimeter (ECAL), and a brass and scintillator hadron calorimeter, each composed of a barrel and two endcap sections. Forward calorimeters extend the pseudorapidity (η) coverage provided by the barrel and endcap detectors. Muons are reconstructed using gas-ionization detectors embedded in the steel flux-return yoke outside the solenoid. Events of interest are selected using a two-tiered trigger system. The first level (L1), composed of custom hardware processors, uses information from the calorimeters and muon detectors to select events at a rate of around 100 kHz within a fixed latency of about 4 μs [29]. The second level, known as the high-level trigger, consists of a farm of processors running a version of the full event reconstruction software optimized for fast processing and reduces the event rate to around 1 kHz before data storage [30]. A more detailed description of the CMS detector, together with a definition of the coordinate system used and the relevant kinematic variables, can be found in Ref. [31].

3 Event reconstruction

The reconstruction of the pp collision products is based on the particle-flow (PF) algorithm [32], which combines information from all CMS subdetectors to reconstruct a set of particle candidates (PF candidates), identified as charged and neutral hadrons, electrons, photons, and muons. The primary vertex (PV) is taken to be the vertex corresponding to the hardest scattering in the event, evaluated using tracking information alone, as described in Ref. [33]. Secondary vertices, which are displaced from the PV, might be associated with decays of long-lived particles emerging from the PV. Any other collision vertices in the event are associated with additional, mostly soft, inelastic pp collisions, referred to as pileup (PU). In the 2016 (2017–2018) datasets, the average number of PU pp collisions was 23 (32).

Electrons are reconstructed using tracks from hits in the tracking system and calorimeter deposits in the ECAL [34]. To increase their purity, reconstructed electrons are required to pass a multivariate electron identification discriminant, which combines information on track quality, shower shape, and kinematic quantities. For this analysis, a working point with an identification efficiency of 90% is used, for a rate of jets misidentified as electrons of $\approx$1%. Muons in the event are reconstructed by combining the information from the tracker and the muon detectors [35]. The mere presence of hits in the muon detectors leads to a strong suppression of particles misidentified as muons. Additional identification requirements on the track fit quality and the compatibility of individual track segments with the fitted track can reduce the misidentification rate further. For this analysis, muon identification requirements with an efficiency of $\approx$99% are chosen, with a misidentification rate below 0.2% for hadrons.

The contributions from backgrounds to the electron and muon selections are further reduced by requiring the corresponding lepton to be isolated from any hadronic activity in the detector. This property is quantified by an isolation variable

$$I_{\text{rel}}^{\text{e}(\mu)} = \frac{1}{p_{\text{T}}^{\text{e}(\mu)}} \left(\sum p_{\text{T}}^{\text{charged}} + \max \left(0, \sum E_{\text{T}}^{\text{neutral}} + \sum E_{\text{T}}^{\gamma} - p_{\text{T}}^{\text{PU}} \right) \right), \tag{1}$$

where $p_{\mathrm{T}}^{\mathrm{e}(\mu)}$ corresponds to the electron (muon) p_{T} and $\sum p_{\mathrm{T}}^{\mathrm{charged}}$, $\sum E_{\mathrm{T}}^{\mathrm{neutral}}$, and $\sum E_{\mathrm{T}}^{\gamma}$ to the p_{T} (or transverse energy E_{T}) sum of all charged particles, neutral hadrons, and photons, in a predefined cone of radius $\Delta R = \sqrt{(\Delta\eta)^2 + (\Delta\varphi)^2}$ around the lepton direction at the PV, where $\Delta\eta$ and $\Delta\varphi$ (measured in radians) correspond to the angular distances of the particle to the lepton in the η and azimuthal angle φ directions. The chosen cone size is $\Delta R = 0.3$ (0.4) for electrons (muons). The lepton itself is excluded from the calculation. To mitigate any distortions from PU, only those charged particles whose tracks are associated with the PV are included. Since an unambiguous association with the PV is not possible for neutral hadrons and photons, an estimate of the contribution from PU ($p_{\mathrm{T}}^{\mathrm{PU}}$) is subtracted from the sum of $\sum E_{\mathrm{T}}^{\mathrm{neutral}}$ and $\sum E_{\mathrm{T}}^{\gamma}$. This estimate is obtained from the mean energy flow in the case of $I_{\mathrm{rel}}^{\mathrm{e}}$ and from tracks not associated with the PV in the case of I_{rel}^{μ}. For negative values, the neutral part of I_{rel} is set to zero.

For each event, hadronic jets are clustered from the PF candidates using the infrared and collinear safe anti-k_{T} algorithm [36, 37] with a distance parameter of 0.4. Jet momentum is determined as the vector sum of all particle momenta in the jet, and is found from simulation to be, on average, within 5 to 10% of the true momentum over the whole p_{T} spectrum and detector acceptance. Pileup can contribute extraneous tracks and calorimetric energy depositions to the jet momentum measurement. To mitigate this effect, charged particles identified to be originating from pileup vertices are discarded and an offset correction is applied to account for the remaining contributions. Jet energy corrections are derived from simulation to bring the measured response of jets to that of particle level jets on average. In situ measurements of the momentum balance in dijet, photon + jet, Z + jet, and multijet events are used to account for any residual differences in the jet energy scale between data and simulation [38]. The jet energy resolution amounts typically to 15–20% at 30 GeV, 10% at 100 GeV, and 5% at 1 TeV [38]. Additional selection criteria are applied to each jet to remove jets potentially dominated by anomalous contributions from various subdetector components or reconstruction failures.

To identify jets resulting from the hadronization of b quarks (b jets) the DeepJet algorithm is used, as described in Refs. [27, 39]. In this analysis, a working point of this algorithm is chosen that corresponds to a b jet identification efficiency of ≈80% for a misidentification rate for jets originating from light-flavour quarks or gluons of $\mathcal{O}(1\%)$ [40]. Jets with $p_{\mathrm{T}} > 30\,\mathrm{GeV}$ and $|\eta| < 4.7$, and b jets with $p_{\mathrm{T}} > 20\,\mathrm{GeV}$ and $|\eta| < 2.4$ are used in the analysis of the 2016 data. From 2017 onwards, after the upgrade of the silicon pixel detector, the b jet η range is extended to $|\eta| < 2.5$.

Jets are also used as seeds for the reconstruction of τ_{h} candidates. This is done by utilizing the features of the PF candidates within the distance parameter of jets using the "hadrons-plus-strips" algorithm, as described in Refs. [26, 41]. Decays to one or three charged hadrons with up to two neutral pions with $p_{\mathrm{T}} > 2.5\,\mathrm{GeV}$ are used (referred to as τ_{h} decay mode thereafter). Neutral pions are reconstructed as strips with dynamic size in η-ϕ from reconstructed photons and electrons contained in the seeding jet, where the electrons originate from photon conversions. The strip size varies as a function of the p_{T} of the electron or photon candidates. The τ_{h} decay mode is then obtained by combining the charged hadrons with the strips. To distinguish τ_{h} candidates from jets originating from the hadronization of quarks or gluons, and from electrons or muons, the DeepTau [26] (DT) algorithm is used. This algorithm uses information from the event, such as tracking, impact parameter, calorimeter cluster composition, and the kinematic and object identification properties of the PF candidates in the vicinity of the τ_{h} candidate, as well as quantities that estimate the PU density of the event. This process results in a multiclassification output y_{α}^{DT} ($\alpha = \tau$, e, μ, jet) that quantifies compatibility of τ_{h} candidate

with the hypothesis of a genuine τ lepton, an electron, a muon, or the hadronization of a quark or gluon. From this output, three discriminants are built according to

$$D_\alpha = \frac{y_\tau^{\mathrm{DT}}}{y_\tau^{\mathrm{DT}} + y_\alpha^{\mathrm{DT}}}, \quad \alpha = \mathrm{e},\ \mu,\ \mathrm{jet}. \tag{2}$$

For the analysis presented here, predefined thresholds on the D_e, D_μ and D_jet discriminants corresponding to the medium working point of the DeepTau algorithm [26] are chosen depending on the $\mathrm{h} \to \tau\tau$ final state, for which the τ_h selection efficiencies and misidentification rates are given in Table 1. The $\mathrm{Z} \to \tau\tau$ decay is used to measure the τ_h identification efficiency. Samples of $\mathrm{Z} \to \mathrm{ee}$ and $\mathrm{Z} \to \mu\mu$ decays are employed to measure the $\mathrm{e} \to \tau_\mathrm{h}$ and $\mu \to \tau_\mathrm{h}$ misidentification rates, respectively. Samples of $\mathrm{W}(\to \ell\nu) + \mathrm{jets}$ events and top quark-antiquark pairs are used to measure the $\mathrm{jet} \to \tau_\mathrm{h}$ misidentification rate.

While neutrinos cannot be detected directly, they contribute to the missing transverse momentum. The missing transverse momentum vector $\vec{p}_\mathrm{T}^{\,\mathrm{miss}}$ is computed as the negative vector sum of the transverse momenta of all the PF candidates in an event [42]. The $\vec{p}_\mathrm{T}^{\,\mathrm{miss}}$ is modified to account for corrections to the energy scale of the reconstructed jets in the event. With $p_\mathrm{T}^{\mathrm{miss}}$ we refer to the magnitude of this quantity.

Table 1: Efficiencies for the identification of τ_h decays and corresponding misidentification rates (given in parentheses) for the working points of D_e, D_μ, and D_jet, chosen for the $\mathrm{h} \to \tau\tau$ selection, depending on the $\tau\tau$ final state. The numbers are given as percentages. Efficiencies and misidentification rates are determined from dedicated studies [26].

$\tau\tau$ channel	D_e (%)	D_μ (%)	D_jet (%)
$\mathrm{e}\tau_\mathrm{h}$	>80 (<0.5)	>99 (<0.5)	>65 (1–3)
$\mu\tau_\mathrm{h}$	>95 (1–2)	>97 (<0.1)	>65 (1–3)
$\tau_\mathrm{h}\tau_\mathrm{h}$	>95 (1–2)	>99 (<0.5)	>65 (1–3)

The mass of the A boson candidate is reconstructed using the FastMTT algorithm [25], which uses a simplified mass likelihood function to reduce the computation time. This algorithm makes use of $\vec{p}_\mathrm{T}^{\,\mathrm{miss}}$ and its uncertainty, and the four-vectors of the reconstructed visible τ lepton decay products to calculate an estimate of the mass of the parent boson and the full four-momenta of the h decay products. Compared to the SVFit algorithm, the FastMTT algorithm removes the contributions of the leptonic and hadronic τ lepton decay matrix elements to the likelihood function, and assumes that visible τ lepton decay products move collinearly with the original τ lepton momentum. This gives a mass resolution that is similar to that of the SVFit algorithm, but the computation time is reduced by two orders of magnitude. Further improvement in the four-lepton mass resolution for $\mathrm{h} \to \tau\tau$ decays is achieved by imposing the mass constraint $m_{\tau\tau} = m_\mathrm{h} = 125\,\mathrm{GeV}$.

In summary, three mass reconstruction techniques have been studied in the course of this analysis: in the first, the four-lepton mass is computed using the leptons from the Z boson decay and only visible decay products of the τ leptons, denoted $m_{\ell\ell\tau\tau}^{\mathrm{vis}}$. This method yields a mass resolution of 20–30%. In the second, the four-lepton mass is computed using the Z boson decay leptons and the FastMTT-corrected τ lepton four-vectors with no mass constraint, denoted $m_{\ell\ell\tau\tau}^{\mathrm{corr}}$. This method yields a resolution on m_A of 10–15%. In the third, the four-lepton mass is computed with the Z decay leptons and the FastMTT-corrected τ four vectors with a mass constraint of $m_{\tau\tau} = 125\,\mathrm{GeV}$ imposed, denoted $m_{\ell\ell\tau\tau}^{\mathrm{cons}}$. This method yields the best experimental resolution on m_A of 5–7% and eliminates the bias in the mean value of the reconstructed mass observed with the other two methods.

These strategies are compared in Fig. 2, where all final states of the A boson decay are combined and the distributions are obtained after applying a selection of $Z \to \ell^+\ell^-$ and $h \to \tau\tau$ candidates, as described in Section 5. The analysis employs the second method to obtain the best estimate for the mass of the h candidate from the FastMTT-corrected four vectors of τ candidates, $m_{\tau\tau}^{\text{corr}}$. This variable is used in the event selection, as described in Section 5. The third method is used to reconstruct the mass of A candidate, $m_{\ell\ell\tau\tau}^{\text{cons}}$. This observable serves as a final discriminant in the statistical inference.

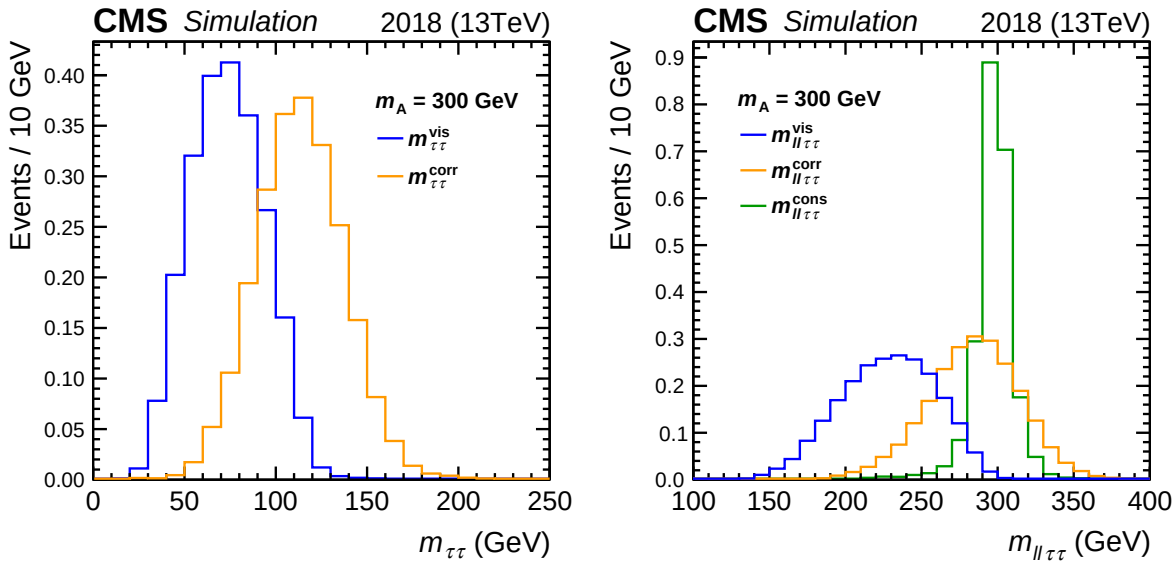


Figure 2: The distribution of the reconstructed mass of the $h \to \tau\tau$ candidate (left plot) and of the $A \to Zh \to (\ell\ell)(\tau\tau)$ candidate (right plot) in a 2018 simulated sample of $gg \to A$ events with $m_A = 300\,\text{GeV}$. Several methods of mass reconstruction are compared: 1) using only the visible decay products of τ lepton ($m_{\tau\tau}^{\text{vis}}$ in the left plot and $m_{\ell\ell\tau\tau}^{\text{vis}}$ in the right plot, blue histograms), 2) using the FastMTT algorithm to correct for missing momentum carried away by neutrinos in the τ lepton decays ($m_{\tau\tau}^{\text{corr}}$ in the left plot and $m_{\ell\ell\tau\tau}^{\text{corr}}$ in the right plot, orange histograms), and 3) using the FastMTT algorithm with a mass constraint of 125 GeV for the $h \to \tau\tau$ candidate ($m_{\ell\ell\tau\tau}^{\text{cons}}$ in the right plot, green histogram).

4 Data and simulated samples

The data sample analyzed in this search corresponds to an integrated luminosity of $138\,\text{fb}^{-1}$ from pp collisions at a centre-of-mass energy at 13 TeV, collected with the CMS detector at the LHC.

Simulated signal events with a *CP*-odd Higgs boson A produced in gluon-gluon fusion and associated production with b quarks, decaying to a 125 GeV Higgs boson and a Z boson are generated at leading order (LO) precision in the strong coupling constant α_S using MADGRAPH5_aMC@NLO v2.6.5 [43], assuming a narrow signal width. The generated A boson mass points lie in the range 225 GeV to 1 TeV. The $A \to Zh$ decaying to $\ell\ell\tau\tau$ is simulated with MADSPIN [44]. In the gluon-gluon fusion production mode, up to one additional jet is included in the matrix element calculations, following the MLM matching scheme with parton showers [45].

In the signal event simulation, the value of m_h is set to 125 GeV and the additional *CP*-even H boson, *CP*-odd A boson, and charged Higgs boson masses are assumed to be at least 225 GeV.

The discrete $\mathbb{Z}_2$ symmetry is broken as in the minimal supersymmetric standard model [46], and CP is enforced to be conserved at tree level in the 2HDM Higgs $\mathbb{Z}_2$ sector [12].

The background samples consist of all SM processes with non-negligible yield in the signal region, including those with a 125 GeV Higgs boson present. The Zh, Wh, and $\mathrm{t\bar{t}h}$ processes, in which an h decaying to two τ leptons is generated in association with a Z boson, W boson, or top quark pair, respectively, are generated at next-to-LO (NLO) precision in α_S with POWHEG v2.0 [47–52]. The contribution from processes with a h boson decaying to two W bosons, produced via Wh or Zh, are generated at NLO precision in α_S using POWHEG and JHUGEN v7.7.2 [53] programs. Contributions from h produced via gluon-gluon fusion or vector boson fusion, where the h decays to two τ leptons or two W bosons, is negligible. The h boson samples are normalized to their inclusive cross sections, and the branching fractions used are those recommended by the LHC Higgs Working Group [54], assuming an m_h mass of 125.38 GeV [10].

The $\mathrm{gg} \to \mathrm{ZZ}$ process is generated at LO precision in α_S with MCFM v7.0.1 [55]. The $\mathrm{q\bar{q}} \to \mathrm{VV}$ processes, where V is either a W or a Z boson, are generated with NLO precision in α_S using POWHEG [56] or with MADGRAPH5_aMC@NLO with the FxFx jet matching and merging scheme [57].

Triboson, $\mathrm{Z}+$jets, $\mathrm{t\bar{t}W}$, and $\mathrm{t\bar{t}Z}$ production are generated via MADGRAPH5_aMC@NLO, with the scheme applied either at NLO precision in α_S exploiting the FxFx jet matching and merging scheme, or at LO precision in α_S with the MLM jet matching and merging scheme. For $\mathrm{Z}+$jets, supplementary samples are generated with up to four outgoing partons in the hard interaction to increase the number of simulated events in regions of high signal purity. The $\mathrm{t\bar{t}}$ background processes is generated at NLO precision in α_S with POWHEG [58]. The $\mathrm{gg} \to \mathrm{ZZ}$, $\mathrm{q\bar{q}} \to \mathrm{VV}$, triboson, $\mathrm{Z}+$jets, $\mathrm{t\bar{t}}$, $\mathrm{t\bar{t}W}$, and $\mathrm{t\bar{t}Z}$ are normalized to their cross sections at NLO precision in α_S or higher [55, 59–64].

For all simulated samples, the NNPDF3.1 [65] parton distribution functions (PDFs) are used for the simulation. Parton showering and hadronization, as well as the τ lepton decays, are modeled using version 8.230 of the PYTHIA event generator [66]. The description of the underlying event is parameterized according to the CP5 [67] tunes for the simulation. Additional inclusive inelastic pp collisions generated with PYTHIA are added according to the expected pileup profile in data. All generated events are passed through a GEANT4-based [68] simulation of the CMS detector and reconstructed using the same version of the CMS event reconstruction software used for the data. The details of the various generator and simulation programs used are summarized in Table 2.

Table 2: Summary of Monte Carlo programs and their purposes.

Program	Version / Scheme	Role / Process Simulated
MADGRAPH5_aMC@NLO	v2.6.5 (LO, MLM)	Signal production ($\mathrm{gg} \to \mathrm{A}, \mathrm{b\bar{b}A}$), narrow-width approximation
MADSPIN	—	Decay of τ leptons with proper spin correlations
POWHEG	v2.0 (NLO)	Zh, Wh, $\mathrm{t\bar{t}h}$ and $\mathrm{t\bar{t}}$ backgrounds at NLO in α_S
JHUGEN	v7.7.2 (NLO)	Wh/Zh with $\mathrm{h} \to \mathrm{WW}^{(*)}$ at NLO, including spin effects
MCFM	v7.0.1 (LO)	$\mathrm{gg} \to \mathrm{ZZ}$ continuum background at LO
MADGRAPH5_aMC@NLO	FxFx (NLO)	$\mathrm{q\bar{q}} \to \mathrm{VV}$ diboson backgrounds at NLO with jet matching
MADGRAPH5_aMC@NLO	MLM (LO)	Triboson, $\mathrm{Z}+$jets, $\mathrm{t\bar{t}W}$, $\mathrm{t\bar{t}Z}$ ($\mathrm{Z}+$jets also with ≤ 4 partons)
PYTHIA	v8.230 (CP5 tune)	Parton shower, hadronization, τ decays
NNPDF3.1	—	Parton distribution functions for all samples
GEANT4	—	Full CMS detector simulation and event reconstruction

5 Event selection

Events are selected online using single-lepton triggers targeting leptons resulting from Z boson decays. The nominal online p_T thresholds for the single-electron (single-muon) trigger are 25–35 GeV (24–27 GeV), depending on the data-taking period. Events are selected if either of the two leptons assigned to a $Z \to ee$ ($Z \to \mu\mu$) decay satisfies the single-electron (single-muon) trigger. The offline p_T selection of the triggering lepton is required to be 1 GeV higher than the nominal p_T threshold of the corresponding trigger. Leptons selected by the trigger are required to geometrically match with a selected offline lepton. Corrections are applied to account for small differences in the trigger selection efficiencies measured in simulation and data.

The light leptons and the τ_h candidates that do not pass the online triggers selections are required to have $p_T > 10$ GeV and $p_T > 20$ GeV, respectively. Constraints on $|\eta|$ arising from detector geometry are $|\eta^e| < 2.5$ for electrons, $|\eta^\mu| < 2.4$ for muons, and $|\eta^{\tau_h}| < 2.3$ for τ_h candidates. These constraints are applied to all selected electrons and muons of the event whether or not they pass the online trigger criteria. The light leptons in an event are required to be separated from each other by $\Delta R > 0.3$, while the τ_h candidates must be separated from each other and from any other lepton by $\Delta R > 0.5$. The resulting selected events are made mutually exclusive by discarding events that have additional identified and isolated electrons or muons.

The Z boson candidates are reconstructed from pairs of same-flavour and opposite-charge light leptons satisfying $60 < m_{\ell^+\ell^-} < 120$ GeV. In events with multiple Z boson candidates, we choose the one with the mass closest to the Z boson mass. The leptons associated with the $h \to \tau\tau$ decay ($e\tau_h$, $\mu\tau_h$, $\tau_h\tau_h$) are required to have opposite charge and an isolation requirement of $I_{rel}^{e(\mu)} < 0.15$, whereas other identification requirements are described in Section 3. The τ_h candidates associated with the h boson must satisfy the τ_h identification with efficiencies detailed in Table 1. In the following, the light lepton (e or μ) and τ_h identification criteria described above are referred to as 'nominal' lepton identification criteria.

Events with at least one identified b jet, according to the criteria given in Section 3, fall into the *b-tag* category, used to target b quark associated A boson production. All other events are placed into the *no b-tag* category, which is used to target gluon-gluon fusion production of the A boson.

To further improve search sensitivity, the FastMTT algorithm is employed to account for unmeasured momentum carried away by τ decay neutrinos. The FastMTT-corrected mass of the $h \to \tau\tau$ candidate, $m_{\tau\tau}^{corr}$, is required to be within the 90–160 GeV mass range.

6 Modeling of signal and background

Backgrounds with prompt lepton decays (ZZ, $t\bar{t}Z$, triboson, and SM processes producing a h boson), and the acceptance of signal processes ($gg \to A$ and $b\bar{b}A$) are estimated from simulation. Background processes are scaled by their theoretical cross sections calculated at the highest order available, as described in Section 4, whereas normalizations of signal processes are extracted from fits to data as described in Section 8.

Reducible background, arising from the misidentification of one or both τ candidates, is estimated from data. The dominant contributions come from the $t\bar{t}$, Z + jets, and WZ + jets processes, where at least one τ candidate is mimicked by a hadronic jet. This background is evaluated using a "misidentification factor" method, that involves measuring the probabilities of misidentifying a hadronic jet as a prompt light lepton or τ_h candidate. The misidentification factors for electrons, muons, and τ_h are measured in a control region dominated by nonprompt

or misidentified leptons, and are defined as the fraction of objects passing the nominal selections in the sample of objects passing loose selections. When selecting signal candidate events, any events with τ candidates passing loose criteria but failing the nominal criteria are assigned to an application region (AR). They are used along with the misidentification factors to estimate the contribution from the reducible background in the signal region, i.e., the region that contains events with leptons or τ_{h} passing identification and isolation. The nominal selection uses the standard criteria defined in Table 1 for identifying events in the signal region, while the loose selection applies only basic requirements and more relaxed criteria.

Loose identification criteria imposed on leptons are summarized in the following.

- Muon candidates: loosened quality criteria on the muon track and relaxed cut on the relative isolation variable (see Eq. 1), $I_{\mathrm{rel}(\mu)} < 0.5$.
- Electron candidates: relaxed cut on the relative isolation variable, $I_{\mathrm{rel}(e)} < 0.5$, and loosened cut on the electron multivariate discriminant.
- τ_{h} candidates : loosened cut on D_{jet} discriminant (see Eq. 2).

Loose identification criteria lead to an increase in the lepton misidentification rate by one to three orders of magnitude, depending on the lepton flavor (e, μ, or τ_{h}), lepton p_{T} and η, and for τ_{h} also on the decay mode.

An estimate of the background from misidentified leptons and τ_{h} in the signal region is obtained by applying suitably chosen weights to the events selected in the AR. Applied weights are computed according to the following relations:

$$\begin{aligned} w_1 &= \frac{f_1}{1-f_1}, \\ w_2 &= \frac{f_2}{1-f_2}, \\ w_{12} &= -\frac{f_1 f_2}{(1-f_1)(1-f_2)}, \end{aligned} \tag{3}$$

where: weight w_1 (w_2) is applied to events where the first (second) τ candidate fails the nominal identification criteria, whereas the second (first) τ candidate passes the nominal identification criteria; weight w_{12} is applied to events where both τ candidates fail the nominal identification criteria; and f_1 and f_2 are the misidentification factors of the first and second τ candidates. The τ candidates are sorted by descending visible transverse momentum, with the leading candidate defined as the 'first' and the subleading as the 'second'. The negative sign of the weight w_{12} accounts for double counting of events from $\mathrm{t\bar{t}}$ and $\mathrm{Z}+\mathrm{jets}$ processes with both τ candidates failing the nominal identification criteria.

The misidentification factors f_i are measured in event samples that have no overlap with the signal region. A validation region, defined to be orthogonal to the signal and measurement regions, is used to test the robustness of the reducible background estimate. Systematic uncertainties corresponding to the possible differences between the true and estimated reducible background rates in the signal region are estimated from these closure tests.

The reducible background estimate involves four regions: the control region enriched in Drell–Yan (DY) events (used to measure misidentification factors), the application region (events failing one or two τ ID criteria and used for applying fake-rate weights), the validation region (same-sign τ candidates used to test the method), and the signal region (events with two τ candidates passing the nominal ID). A summary of the definitions and purposes of all control regions discussed in this Section, along with the definition of the signal region, is provided in

Table 3. It should be noted that the selection criteria defining the regions listed in Table 3 ensure their mutual orthogonality.

The dedicated DY control region requires an additional hadronic jet that is misidentified as a light lepton or a τ_h candidate. This control region is used to measure the misidentification (fake) rates for jets misidentified as τ_h candidates, electrons, or muons. The estimation of misidentification factors relies on reconstructing an opposite-charge, same-flavour lepton pair compatible with a Z boson, and requiring one additional loosely selected lepton or τ_h candidate (i.e., passing an identification working point looser than the one used in the signal region).

The requirements on the leptons originating from the Z boson are the same as those defined in Section 5, but they must fulfil a more stringent dilepton mass cut with $81 < m_{\ell^+\ell^-} < 120\,\text{GeV}$. The lower threshold on the dilepton mass is tightened to suppress the contribution of DY events affected by final-state radiation. These events typically have lower dilepton mass compared to DY events without final-state radiation.

Table 3: Summary of regions used in the misidentification factor method.

Common for all regions	
e^+e^- or $\mu^+\mu^-$ pair consistent with Z decay	
Definition	**Purpose**
Determination region (DR)	
one and only one τ candidate passing loose lepton id.	determination of lepton misidentification factors ($f_{1,2}$ in Eq. 3)
Application region (AR)	
$\tau^+\tau^-$ pair where both τ candidates pass loose lepton id. but at least one fails nominal id.	construction of the reducible background model by applying misidentification factors
Validation region (VR)	
same sign $\tau^\pm\tau^\pm$ pair where both τ canidates pass nominal lepton id.	validation of the reducible background model, assessment of related systematic uncertainties
Signal region (SR)	
$\tau^+\tau^-$ pair where both τ candidates pass nominal lepton id.	selection of events into final sample, where the signal is extracted

After reconstructing the $Z \to \ell^+\ell^-$ candidate, the misidentification factor is estimated by applying the lepton identification algorithm to the additional loosely identified light lepton or τ_h candidate in the event. Orthogonality to the signal region is achieved by rejecting events with extra τ candidates (either light lepton or τ_h), passing loose identification criteria. The misidentification factors are measured in different bins of lepton p_T, and are further split between reconstructed decay modes for the τ_h candidate, and for muons and electrons in bins of lepton η, based on the barrel and endcap regions. The events where the τ candidates are genuine τ_h, electrons, or muons, are estimated from simulation and subtracted from data so that the misidentification factors are measured for genuine hadronic jets only. The misidentification factors obtained for electrons (muons) are <2 (5)% in the barrel and endcap regions for lepton

$p_T > 10\,\text{GeV}$, whereas for τ_h candidates with $p_T > 20\,\text{GeV}$ the misidentification factors vary between 2 and 20%, depending on the decay mode and discriminator working point.

The measured misidentification factors are validated in another region that consists of events with a Z boson candidate and two additional τ candidates. To ensure that the validation region is not contaminated with signal events or contributions from backgrounds with genuine prompt leptons, the two additional τ candidates are required to have the same charge. All other selection criteria are identical to those defining the signal region. The reducible background in the validation region is constructed in the same way as in the nominal analysis. The purity of the reducible background in the validation region amounts to more than 95% in all analyzed channels.

Given the limited statistical power of the data sample in the validation region, the observed data yields and shapes of the $m^{\text{cons}}_{\ell\ell\tau\tau}$ distribution are compared with the predicted yields and shapes of the reducible background by combining all three data-taking periods. The comparison revealed only modest differences between the observed data and the model of the reducible background. The saturated goodness of fit (GoF) test [69], quantifying consistency of the observed data with the background model, yields p-values of 0.31, 0.48, and 0.82 for the $\tau_h\tau_h$, $e\tau_h$, and $\mu\tau_h$ channels, respectively. This test is performed using the CMS statistical toolkit COMBINE [70]. The differences between the observed data and the model, together with the statistical uncertainties due to the limited data sample in the validation region, are accounted for by assigning a systematic uncertainty in the yield of the reducible background, estimated to be 20–30% depending on the h decay channel. Given that the comparison is performed for the combined dataset, these uncertainties are correlated among data-taking periods, but uncorrelated among h decay channels.

The limited statistical power of the data sample in the AR, along with the contribution of events with negative weights (Eq. 3), hampers the construction of smooth templates to model the shape of the $m^{\text{cons}}_{\ell\ell\tau\tau}$ distribution of the reducible background. The shape of the distribution is therefore taken from a data region with same-sign τ candidates that pass loose identification and isolation requirements. This region has higher statistical power than the AR region, resulting in a smoother shape for the $m^{\text{cons}}_{\ell\ell\tau\tau}$ distribution, which is normalized to the estimated yield of the reducible background in the signal region. Consistency of shapes obtained from the statistically limited AR and the region with same-sign τ candidates, passing loose identification criteria, is verified with a Kolmogorov-Smirnov test, yielding p-values between 0.56 and 0.97 depending on the di-τ decay mode.

7 Systematic uncertainties

The dominant systematic uncertainties considered in the analysis are summarized in Table 4.

The uncertainties in the τ_h identification efficiency are estimated in $Z \to \tau\tau$ and $W \to \tau\nu$ decays from control samples. These uncertainties are partially correlated across data-taking years. The size of uncertainties varies in the range of 2–10% per τ_h, depending on p_T and the decay mode of the τ_h candidate [26]. The uncertainties in the τ_h energy scale amount to 0.5–1.1%, depending on the τ_h decay mode. They are predominantly of statistical origin and uncorrelated between data-taking years. Uncertainties in the τ_h identification efficiency and momentum scale affect both the normalization of simulated processes and the shape of the $m^{\text{cons}}_{\ell\ell\tau\tau}$ distribution.

Uncertainties in the identification and isolation efficiencies of electrons and muons are 1.5% and

are correlated across all years. These uncertainties result in normalization variations between 1.5% and 4.5%, depending on the analyzed final state. Uncertainties in the muon momentum scale amount to less than 0.3% and have a negligible impact on the analysis. The uncertainty in the electron energy scale, which is derived from the calibration of the ECAL crystals and applied on an event-by-event basis, is less than 2%. The uncertainty in the single-lepton trigger efficiency results in a normalization uncertainty of about 2% for both single-electron and single-muon triggers.

Uncertainties in both the identification efficiency for b jets and in the misidentification rates for light-flavour or c quarks or gluon jets range from the subpercent level to $\mathcal{O}(10\%)$, depending on jet flavour and p_{T}. The uncertainty in the identification efficiency of b jets causes variation of 1–4% (0.3–1%) in the normalization of the $\mathrm{b\bar{b}A}$ signal and background processes with genuine b jets in the *b-tag* (*no b-tag*) category. The uncertainty in the misidentification efficiency of the light-flavour, or c quarks, or gluon jets modifies normalization of the $\mathrm{gg} \to \mathrm{A}$ signal and background processes with no genuine b jets by 5–10% in the *b-tag* category and has an impact of $\mathcal{O}(0.1\%)$ on the normalization of processes without genuine b jets in the *no b-tag* category.

An uncertainty related to the energy carried by unclustered particle candidates, which are not contained in jets in the event [42], is propagated on an event-by-event basis to $p_{\mathrm{T}}^{\mathrm{miss}}$, resulting in a variation of up to 10% in the shape of the $m_{\ell\ell\tau\tau}^{\mathrm{cons}}$ distribution. A normalization-altering effect of 1–3% is introduced by this uncertainty by requiring $90 < m_{\tau\tau}^{\mathrm{corr}} < 160\,\mathrm{GeV}$. The jet energy scale and resolution affect both the selection efficiencies and shapes of the $m_{\ell\ell\tau\tau}^{\mathrm{cons}}$ distributions. The jet energy scale is responsible for a 1–3% variation in the number of selected background and signal events; the jet energy resolution contributes an additional 0.5–1%. The calibration accuracy of the unclustered and jet energy scales and jet energy resolution is mainly affected by statistical limitations of the measurements, the time-dependence of the data-taking conditions, and the aging of the detector. For this reason, the respective uncertainties are uncorrelated between data-taking years.

Theoretical uncertainties related to the choice of PDFs, and the renormalization (μ_{R}) and factorization (μ_{F}) scales, affecting both the acceptance and cross section of the dominant background processes, are estimated from simulation separately for each process. Uncertainties due to the choice of μ_{R} and μ_{F} in the calculation of the matrix elements are obtained from an independent variation of these scales by factors of 0.5 and 2, omitting the variations where one scale is multiplied by 2 and the corresponding other scale by 0.5. The uncertainties are then obtained from an envelope of these variations. The uncertainties due to PDF variations and the uncertainty in α_{S} are obtained following the PDF4LHC recommendations [71], taking the root mean square of the variation of the results when using different replicas of the default NNPDF3.1 set.

Combining μ_{R} and μ_{F} scale uncertainties with the PDF set uncertainty for the $\mathrm{q\bar{q}} \to \mathrm{ZZ}$ process leads to a normalization uncertainty of 5%. For the $\mathrm{gg} \to \mathrm{ZZ}$ process, a normalization uncertainty of 15% is obtained. It covers variations of μ_{R} and μ_{F}, PDF set and α_{S} uncertainties, and uncertainty that accounts for effects of interference with the process mediated by the off-shell Higgs boson, $\mathrm{gg} \to \mathrm{h}^* \to \mathrm{ZZ}$ [9, 59]. The uncertainties in cross sections of the $\mathrm{t\bar{t}Z}$ and triboson production amount to 25% [72] and dominate normalization uncertainty for these processes.

The uncertainty in the theoretical calculations of the SM $\mathrm{h} \to \tau\tau$ branching fraction, amounting to 2% [54] is applied to both the signal samples as well as all backgrounds that include the $\mathrm{h} \to \tau\tau$ process. The inclusive uncertainty for Zh production related to the PDFs amounts to 1.3%, whereas the uncertainty for the variation of μ_{R} and μ_{F} is 0.9% [54]. For the subleading h boson processes $\mathrm{gg} \to \mathrm{h} \to \mathrm{ZZ}$, and $\mathrm{t\bar{t}h}$ the inclusive uncertainties related to the PDFs amount to 3.2 and 3.6% and the uncertainties for the variation of μ_{R} and μ_{F} are 3.9 and 8%,

respectively [54].

For the MSSM parameter scan, theoretical uncertainties in the $gg \to A$ and $b\bar{b}A$ cross sections are accounted for as described in Ref. [73]. This includes uncertainties in μ_R, μ_F, PDFs, and α_S. Uncertainties are evaluated separately for each m_A-tan β point under consideration. They are typically 5–20% (10–25%)) for $gg \to A$ ($b\bar{b}A$) production.

Uncertainties in the estimated yield of background with misidentified leptons comprise two components. Statistical uncertainties arise from the limited statistical power of the data sample in the AR. These are the dominant uncertainties in the analysis and they range between 10–20% (20–40%) in the *no b-tag* (*b-tag*) category and are uncorrelated between channels, event categories, and data-taking periods. Uncertainties related to the misidentification factor method are estimated in the sideband region with same-sign τ pairs, as described in Section 6. Normalization uncertainties of 20–30% are assigned to the estimated yield of this background. They are correlated between data-taking periods and event categories but uncorrelated across di-τ final states.

The integrated luminosities of the 2016, 2017, and 2018 data-taking periods are known with uncertainties in the 1.2–2.5% range [74–76], while the total integrated luminosity for the years 2016–2018 has an uncertainty of 1.6%. Uncertainties related to the finite number of simulated events, referred to in Table 4 as bin-by-bin statistical uncertainties, are taken into account using the Barlow-Beeston "lite" method [70, 77, 78]. They are considered for all bins of the distributions used to extract the results. They are uncorrelated across different samples and across bins of a single distribution.

The uncertainty in the predicted yield of the reducible background and theoretical uncertainties in cross sections of the $q\bar{q} \to ZZ$, $gg \to ZZ$, and $t\bar{t}Z$ processes are the dominant factors limiting the sensitivity of the search. Their combined effect reduces sensitivity of the analysis by 15–20% (20–25%) in terms of expected upper limits on the rate of the $gg \to A$ ($b\bar{b}A$) process.

8 Results

The discriminating variable for this analysis is $m^{\text{cons}}_{\ell\ell\tau\tau}$, the mass of the four-lepton final state where four-vector of the $h \to \tau\tau$ candidate is reconstructed by the FastMTT algorithm [25] with the mass constraint $m_{\tau\tau} = 125\,\text{GeV}$. Six final states corresponding to each combination of $Z \to ee, \mu\mu$ and $h \to e\tau_h, \mu\tau_h, \tau_h\tau_h$ decays are considered. Each final state comprises two event categories, *no b-tag* and *b-tag*, as described in Section 5. Data are examined for the presence of signal using the CMS statistical analysis toolkit COMBINE [70], which is based on the ROOFIT [79] and ROOSTATS [80] frameworks.

The signal extraction is performed with a simultaneous binned likelihood fit, combining 36 $m^{\text{cons}}_{\ell\ell\tau\tau}$ distributions, which correspond to 6 analyzed final states times 2 event categories times 3 data-taking periods. The likelihood used to infer the signal has the following form:

$$\mathcal{L}\left(\{k_i\},\{\mu_s\},\{\theta_j\}\right) = \prod_i \mathcal{P}\left(k_i \middle| \sum_s \mu_s S_{si}(\{\theta_j\}) + \sum_b B_{bi}(\{\theta_j\})\right) \prod_j \mathcal{C}(\widetilde{\theta}_j|\theta_j), \tag{4}$$

where μ_s denotes the value of the signal strength modifier associated with the signal s (either $gg \to A$ or $b\bar{b}A$) that maximizes the likelihood function (i.e., the best-fit signal strength), with the signal strength modifier defined as the ratio between the measured signal rate and the rate assumed for the signal model. Furthermore, i labels the bins of the discriminating distributions, split by the final state, signal category (*no b-tag* or *b-tag*), and data-taking year. The function

Table 4: Dominant sources of systematic uncertainty are considered in this analysis. The symbol † indicates uncertainties that affect both the shape and normalization of the final $m_{\ell\ell\tau\tau}^{\text{cons}}$ distributions. Uncertainties without † affect only normalization. The magnitude column indicates an approximation of the associated change in normalization. The uncertainties in each group are listed in descending order of their impact on the analysis sensitivity.

Source of uncertainty	Magnitude	Process
Experimental uncertainties		
τ_h id.†	2–10%	all simulations
μ trigger	2%	all simulations
μ id. & isolation	1.5–4.5%	all simulations
e trigger	2%	all simulations
e id. & isolation	1.5–4.5%	all simulations
limited MC event count	bin-by-bin uncertainties	all simulations
τ_h energy scale†	0.5–1.5%	all simulations
integrated luminosity	<2%	all simulations
e energy scale†	1–2%	all simulations
b jet identification efficiency	1–4%	all simulations
b jet misidentification rate	5–10%	all simulations
jet energy scale†	1–3%	all simulations
$\vec{p}_T^{\,\text{miss}}$ unclustered energy scale†	1–3%	all simulations
jet energy resolution†	<1%	all simulations
Uncertainties in reducible background estimate		
		misidentified τ leptons
normalization uncertainty	30%	eτ_h channel
	20%	$\mu\tau_h$ channel
	20%	$\tau_h\tau_h$ channel
event count in AR	20–40%	(*b-tag* category)
	10–20%	(*no b-tag* category)
Theoretical uncertainties in background estimate		
$q\bar{q} \to ZZ$ normalization	5%	$q\bar{q} \to ZZ$
$gg \to ZZ$ normalization	15%	$gg \to ZZ$
$t\bar{t}Z$ normalization	25%	$t\bar{t}Z$
triboson normalization	25%	triboson
μ_F and μ_R scales	1–8%	Higgs bkg.
theoretical uncertainty in $\mathcal{B}(h \to \tau\tau)$	<2%	$gg \to A$, $b\bar{b}A$, Higgs bkg.
PDFs	1.3–3.6%	Higgs bkg.
Theoretical uncertainties in the signal estimate (applied in the MSSM interpretation)		
signal cross section		
(μ_F, μ_R scale, PDFs, α_S)	5–20% (10–25%)	$gg \to A$ ($b\bar{b}A$)

$\mathcal{P}(k_i|\sum \mu_s S_{si}(\{\theta_j\}) + \sum B_{bi}(\{\theta_j\}))$ corresponds to the Poisson probability to observe k_i events in bin i for a prediction of $\sum \mu_s S_{si}$ signal and $\sum B_{bi}$ background events. The predictions for S_{si} and B_{bi} are obtained from the signal and background models. The parameters μ_s act as linear scaling factors of the corresponding signal s. Systematic uncertainties are incorporated in the form of constraint terms for additional nuisance parameters $\{\theta_j\}$ in the likelihood, appearing as a product with predefined probability density functions $\mathcal{C}(\widetilde{\theta}_j|\theta_j)$, where $\widetilde{\theta}_j$ corresponds to the nominal value for θ_j. The predefined uncertainties in the $\widetilde{\theta}_j$, as discussed in Section 7, may be constrained by the fit to the data.

The test statistic used for the inference of the signal is the profile likelihood ratio as discussed in Ref. [81]:

$$q_{\mu_s} = -2\ln\left(\frac{\mathcal{L}(\{k_i\}|\sum_s \mu_s S_{si}(\{\hat{\theta}_{j,\mu_s}\}) + \sum_b B_{bi}(\{\hat{\theta}_{j,\mu_s}\}))}{\mathcal{L}(\{k_i\}|\sum_s \hat{\mu}_s S_{si}(\{\hat{\theta}_{j,\hat{\mu}_s}\}) + \sum_b B_{bi}(\{\hat{\theta}_{j,\hat{\mu}_s}\}))}\right), \quad 0 \leq \hat{\mu}_s \leq \mu_s, \tag{5}$$

where μ_s are tested values of the parameters of interest (POIs); $\hat{\theta}_{j,\mu_s}$ are the values of the nuisance parameters that maximize the likelihood function for specified values of μ_s, i.e. these are conditional maximum likelihood estimators of θ_j and thus are functions of μ_s; $\hat{\mu}_s$ and $\hat{\theta}_{j,\hat{\mu}_s}$ are unconditional maximum likelihood estimators of POIs and nuisance parameters. The index of q_{μ_s} indicates that the test statistic is evaluated for specified values of μ_s.

Compared to the unbinned approach, the binned likelihood fit does not require the introduction of analytical probability density functions for description of the background and signal models, thereby simplifying statistical inference. The likelihood function is rigorously defined and properly accounts for the analysis bins with zero observed yields. The background and signal models are represented as binned templates derived from simulated samples or the sideband region in data as described in Section 6. The binning has been optimised to maintain high sensitivity in the entire probed range of m_{A} while ensuring reasonable statistical population across all bins of the final discriminant in the combined background template, with the statistical uncertainty ranging between 0.5% and 30%.

The statistical model includes two POIs: the rate of $\mathrm{gg} \to \mathrm{A}$ production and the rate of $\mathrm{b\bar{b}A}$ production. Constraints on the production rates of the signal processes are derived using the modified frequentist $\mathrm{CL_s}$ method [82, 83].

The $m_{\ell\ell\tau\tau}^{\mathrm{cons}}$ distributions, combined across all search channels, are presented in Fig. 3. The distributions are shown separately for *no b-tag* and *b-tag* categories.

Expected and observed event yields in the final selected sample are reported in Table 5.

It should be noted that b jets in the $\mathrm{b\bar{b}A}$ process have a relatively soft p_{T} spectrum, and about two-thirds of $\mathrm{b\bar{b}A}$ events have b jets outside the acceptance of b tagging algorithm. As a consequence, about 75% of selected $\mathrm{b\bar{b}A}$ events contribute to the *no b-tag* category, with the remaining 25% assigned to the *b-tag* category.

The statistical inference did not reveal any evidence for the presence of a signal. The compatibility of the observed distributions of the $m_{\ell\ell\tau\tau}^{\mathrm{cons}}$ discriminant with a null hypothesis is evaluated with a GoF test, confronting data against a background-only expectation. The p-value returned by a GoF test based on the saturated model for the test statistics [69], is 0.89. The results of the analysis are used to constrain the rate of the signal processes. The upper limits at 95% confidence level (CL) on the A production cross section times branching fraction of $\mathrm{A} \to \mathrm{Zh}$ are shown in Fig. 4 for all channels combined. The statistical inference is performed with one

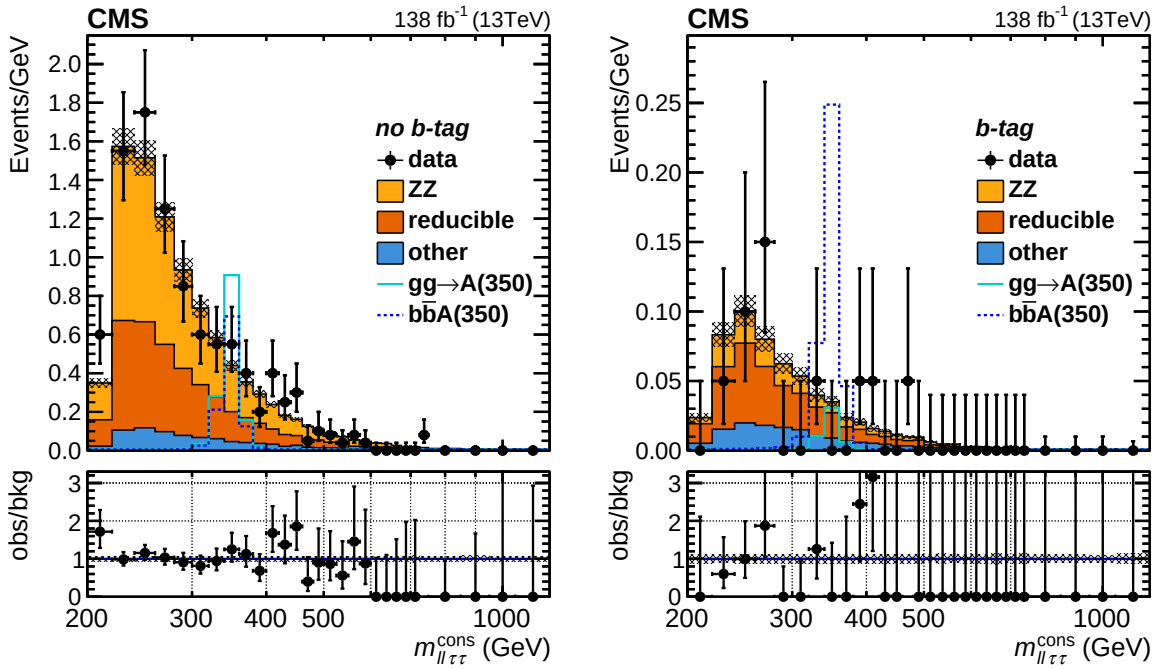


Figure 3: The reconstructed four-lepton mass, $m_{\ell\ell\tau\tau}^{\text{cons}}$, in the *no b-tag* (left plot) and *b-tag* (right plot) categories. Background distributions are shown after performing a maximum likelihood fit to the data under a background-only hypothesis. Signal samples corresponding to the $gg \to A$ and $b\bar{b}A$ production modes of a pseudoscalar Higgs boson with a mass of $m_A = 350\,\text{GeV}$, are overlaid to illustrate the expected signal contribution. Signal yields are computed by setting $\sigma\mathcal{B}(A \to Zh)$ to a benchmark value of 1 pb for both $gg \to A$ and $b\bar{b}A$ processes. Hatched bands indicate uncertainties in the total background. Contents of each bin, along with the corresponding uncertainties, are divided by the bin width.

Table 5: Expected and observed yields in the final selected sample. The $Z \to ee$ and $Z \to \mu\mu$ samples and all three data-taking periods are combined for the final results. Numbers are reported individually for *no b-tag* and *b-tag* categories and three analyzed di-τ decay modes: $e\tau_h$, $\mu\tau_h$, and $\tau_h\tau_h$, combining $Z \to ee$, $\mu\mu$ channels and three data-taking years. Background yields and related uncertainties are obtained after performing a maximum likelihood fit to the data under a background-only hypothesis. Signal yields are computed for representative chosen mass hypotheses of m_A = 250, 350, 500, and 800 GeV, by setting $\sigma\mathcal{B}(A \to Zh)$ to a benchmark value of 1 pb for both the $gg \to A$ and $b\bar{b}A$ processes.

Process	*no b-tag*			*b-tag*		
	$e\tau_h$	$\mu\tau_h$	$\tau_h\tau_h$	$e\tau_h$	$\mu\tau_h$	$\tau_h\tau_h$
ZZ	25.6 ± 3.4	36.4 ± 4.1	41.9 ± 5.2	0.75 ± 0.13	1.09 ± 0.18	1.28 ± 0.21
reducible	18.7 ± 5.2	14.8 ± 3.4	33.5 ± 8.4	3.41 ± 1.09	1.69 ± 0.49	1.21 ± 0.35
other	4.4 ± 1.1	6.6 ± 1.5	7.0 ± 1.5	0.99 ± 0.26	1.43 ± 0.37	0.68 ± 0.17
total bkg.	48.7 ± 6.4	57.8 ± 5.6	82.4 ± 9.9	5.15 ± 1.14	4.21 ± 0.68	3.17 ± 0.47
observed	58	57	81	4	2	4
$gg \to A$ (250 GeV)	4.70	6.84	8.66	0.16	0.24	0.30
$b\bar{b}A$ (250 GeV)	3.70	5.44	7.04	1.24	1.72	2.26
$gg \to A$ (350 GeV)	6.66	9.54	12.36	0.24	0.34	0.44
$b\bar{b}A$ (350 GeV)	5.10	7.34	9.40	1.88	2.64	3.40
$gg \to A$ (500 GeV)	8.94	12.68	16.44	0.38	0.52	0.68
$b\bar{b}A$ (500 GeV)	6.74	9.38	12.38	2.72	3.78	4.98
$gg \to A$ (800 GeV)	11.90	16.76	22.20	0.56	0.76	1.06
$b\bar{b}A$ (800 GeV)	8.72	12.28	16.38	3.82	5.26	7.14

POI, corresponding to the rate of the probed process, whereas the rate of the other process is fixed to zero. This interpretation targets BSM scenarios, where one of the two processes, either $gg \to A$ or $b\bar{b}A$, prevails, whereas the contribution of the other process to the signal is negligible. The example of such scenarios is given by Type-II 2HDM, where at low $\tan\beta$ values the A boson production is dominated by the $gg \to A$ process, while the $b\bar{b}A$ process has vanishing cross section. The branching fraction of the $h \to \tau\tau$ decay is set to the value predicted in the SM, $\mathcal{B}(h \to \tau\tau) = 0.062$ [54]. The observed (expected) limits range from 0.049 (0.060) pb at $m_A = 1$ TeV to 1.02 (0.79) pb at $m_A = 250$ (225) GeV for the $gg \to A$ process. For the $b\bar{b}A$ process, the observed (expected) limits range from 0.053 (0.059) pb at $m_A = 1$ TeV to 0.79 (0.61) pb at $m_A = 250$ (225) GeV.

Results of the search are also provided in terms of two-dimensional constraints on the cross section times branching fraction, $\sigma\mathcal{B}(A \to Zh)$, for the $gg \to A$ and $b\bar{b}A$ production mechanisms. Constraints are derived assuming that the rates of $gg \to A$ and $b\bar{b}A$ processes are nonnegative. Figures 5 and 6 present 68% and 95% CL contours for eight representative m_A hypotheses. For each m_A, $\sigma\mathcal{B}(A \to Zh)$ values are scanned in two dimensions, corresponding to the $gg \to A$ and $b\bar{b}A$ production mechanisms. At each scanned point, $-2\log L$ is calculated, defined as the negative-log-likelihood (NLL) of the conditional fit to the background-only Asimov and observed datasets. The minimal value of the NLL in the scanned domain of nonnegative values of $\sigma(gg \to A)\mathcal{B}(A \to Zh)$ and $\sigma(b\bar{b}A)\mathcal{B}(A \to Zh)$ defines the best fit point. For each scanned point, the difference between the NLL at a given point and the minimal value of NLL, $-2\Delta(\log L)$, is then computed. The 68% and 95% CL boundaries are found at $-2\Delta(\log L)$ val-

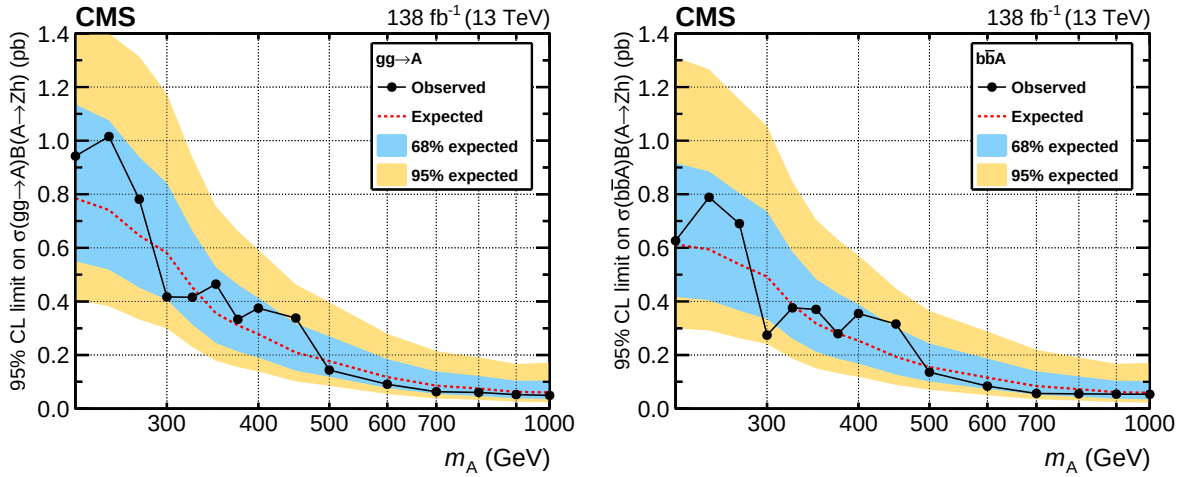


Figure 4: The expected and observed upper limits at 95% CL on the production cross section times branching fraction of the $A \to Zh$ decay for $gg \to A$ (left plot) and $b\bar{b}A$ (right plot) processes as functions of m_A. The limits for the $gg \to A$ ($b\bar{b}A$) process are derived with the rate of other process fixed to zero. The branching fraction of the $h \to \tau\tau$ decay is set to the value predicted in the SM, $\mathcal{B}(h \to \tau\tau) = 0.062$ [54].

ues of 2.30 and 5.99, respectively. Maximum-likelihood fits to the background-only Asimov dataset are performed to extract 68% and 95% CL expected contours in the absence of signal. Fits to data are performed to determine the observed 68% and 95% CL contours.

The results of this analysis are also interpreted as constraints on the parameters $\tan\beta$ and m_A within the $M_{h,EFT}^{125}$ MSSM benchmark scenario [17]. For this scenario the Higgs boson masses, mixing angle α, and effective Yukawa couplings have been calculated with the FEYNHIGGS [84–91] program. Branching fractions for the $A \to Zh$ and $h \to \tau\tau$ decays have been obtained from a combination of the FEYNHIGGS and HDECAY [92] programs, as described in Ref. [73] following the prescriptions given in Refs. [54, 93, 94]. For the $gg \to A$ process the cross sections are obtained with SUSHI 1.7.0 [95, 96], which includes NLO corrections in α_S for the t- and b-quark contributions to the cross section [97, 98], NNLO corrections in α_S in the heavy t quark limit, for the t quark contribution [99–103], and next-to-NNLO contributions in α_S for h production [104–106]. Electroweak corrections mediated by light-flavour quarks are included at two-loop accuracy reweighting the SM results of Refs. [107, 108]. Cross sections for the $b\bar{b}A$ process rely on matched predictions [109–112], which are based on the calculation at NNLO in α_S in the five-flavour scheme [113] and the calculation at NLO in α_S in the four-flavor scheme [114, 115].

At low $\tan\beta$ values, the $A \to Zh$ decay dominates the natural decay width of A in the m_A range from 220 to 350 GeV. For higher values of m_A decays $A \to t\bar{t}$ become dominant. For $\tan\beta \lesssim 4$, the A boson is produced mainly via gluon-gluon fusion process, but at higher $\tan\beta$ values, associated production with bottom quarks takes over.

To derive exclusion contours at 95% CL, a scan in the m_A-$\tan\beta$ plane is performed. Signal yields are determined based on the theoretical predictions for $\sigma(gg \to A)$, $\sigma(b\bar{b}A)$, $\mathcal{B}(A \to Zh)$ and $\mathcal{B}(h \to \tau\tau)$ at a given tested m_A-$\tan\beta$ point, and the CL_s value [83] is computed. Those points where CL_s falls below 5% define the 95% CL exclusion contour for the benchmark scenario under consideration. Observed and expected lower limits at 95% CL on $\tan\beta$ as functions of m_A are presented in Fig. 7. Observed (expected) limits on $\tan\beta$ range from 1.4 (1.5) at $m_A = 375$ GeV to 4.0 (3.9) at $m_A = 325$ GeV. This analysis excludes $\tan\beta$ values below 2.2 at 95% CL in the mass range from 225 to 350 GeV. At higher probed values of m_A, $A \to t\bar{t}$ decay becomes

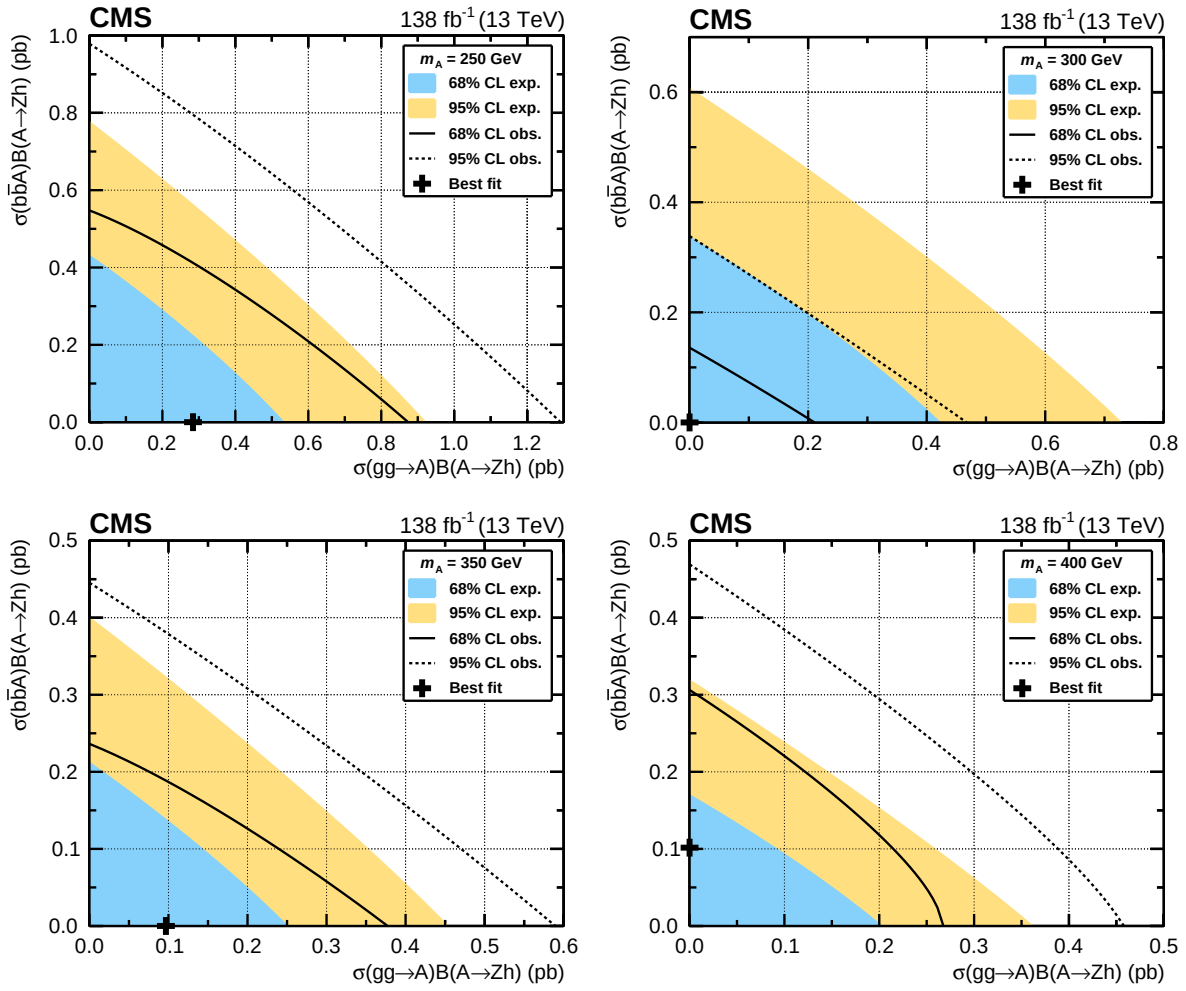


Figure 5: Two-dimensional constraints on the cross section times branching fraction for the two production mechanisms. The confidence level intervals are derived for mass hypotheses of $m_{\mathrm{A}} = 250$ (upper left plot), 300 (upper right plot), 350 (lower left plot), and 400 GeV (lower right plot). The branching fraction of the $\mathrm{h} \to \tau\tau$ decay is set to the value predicted in the SM, $\mathcal{B}(\mathrm{h} \to \tau\tau) = 0.062$ [54]. Computation of the best fit point and determination of the observed and expected 68% and 95% CL contours are described in the text.

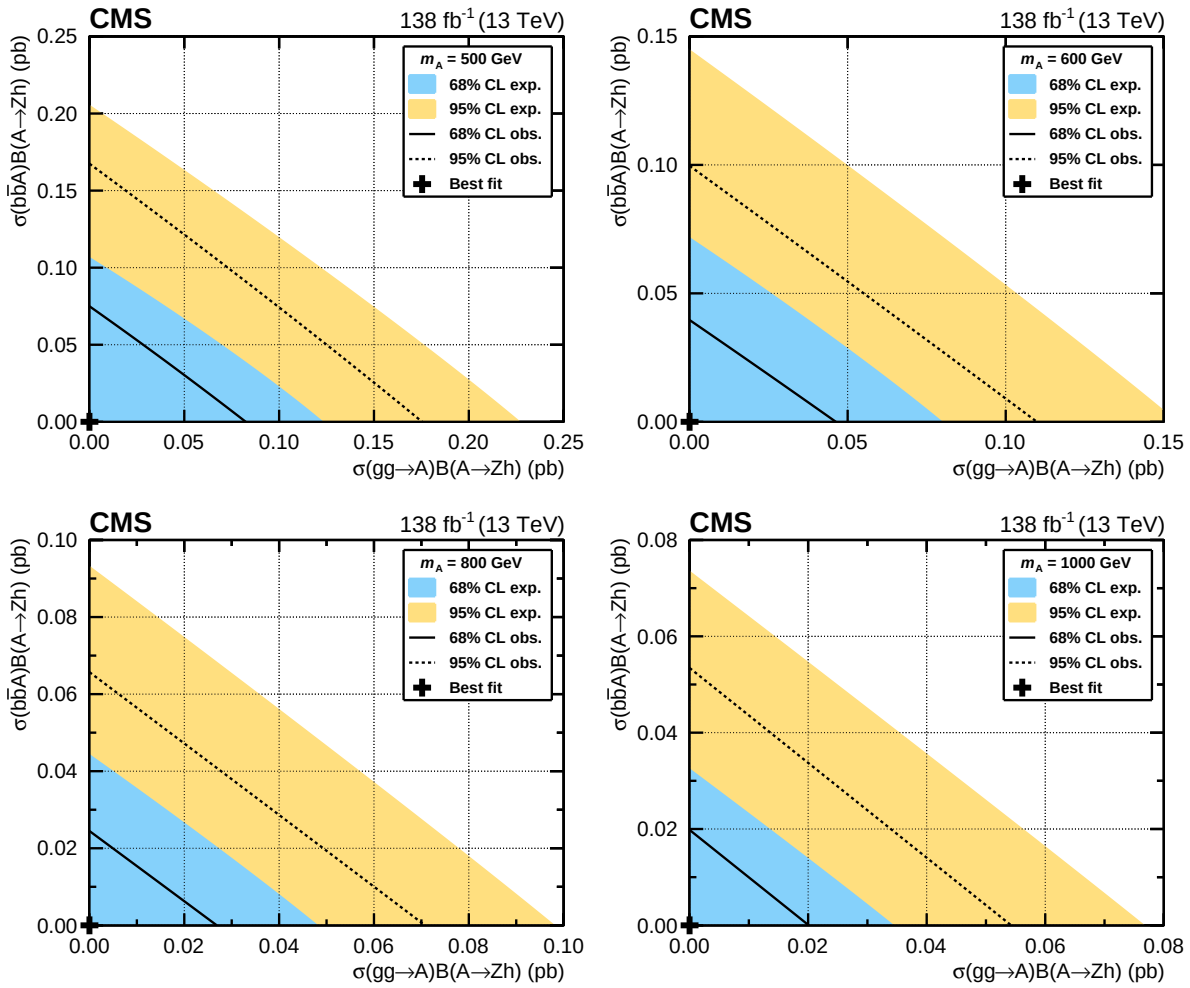


Figure 6: Same as Fig. 5 but for mass hypotheses of $m_{\mathrm{A}} = 500$ (upper left plot), 600 (upper right plot), 800 (lower left plot) and 1000 GeV (lower right plot). The branching fraction of the $\mathrm{h} \to \tau\tau$ decay is set to the value predicted in the SM, $\mathcal{B}(\mathrm{h} \to \tau\tau) = 0.062$ [54]. Computation of the best-fit point and determination of the observed and expected 68% and 95% CL contours are described in the text.

kinematically allowed and suppresses $A \to Zh$ decay, significantly reducing the sensitivity of this search.

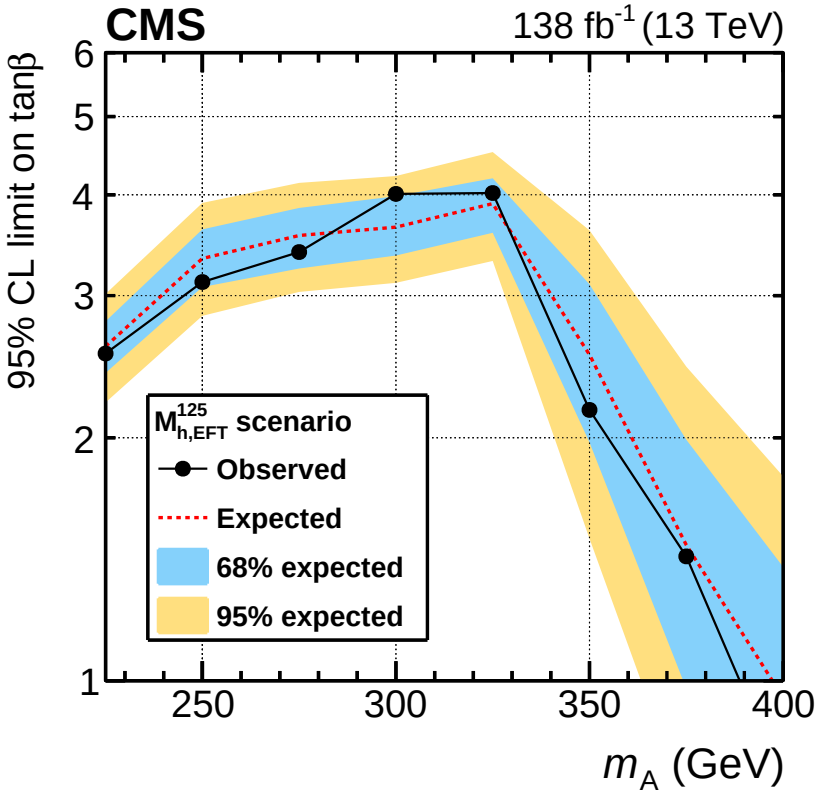


Figure 7: Lower 95% CL limit on $\tan\beta$ as a function of m_A in the $M^{125}_{h,EFT}$ MSSM scenario. Values below the black solid line are excluded at 95% CL.

9 Summary

A search is presented for the decay of a heavy pseudoscalar boson A to a Z boson and a 125 GeV Higgs boson, h, in final states with two τ leptons and two light leptons (ee, $\mu\mu$). The study is based on proton-proton collision data collected by the CMS experiment at $\sqrt{s} = 13$ TeV, corresponding to an integrated luminosity of 138 fb^{-1}. The analysis probes the gluon-gluon fusion process, $gg \to A$, and bottom quark associated production, $b\bar{b}A$. No evidence for a signal is found in the data. Upper limits at 95% confidence level are derived on the product of the cross section and branching fraction of the $A \to Zh$ decay under the assumption that the scalar state h has the properties of the 125 GeV SM Higgs boson. Observed limits range from 0.049 (0.053) pb at $m_A = 1$ TeV to 1.02 (0.79) pb at $m_A = 250$ GeV for the $gg \to A$ ($b\bar{b}A$) process.

The results of the search are also interpreted in terms of constraints on $\tan\beta$ as a function of m_A within the $M^{125}_{h,EFT}$ MSSM benchmark scenario. Values of $\tan\beta$ below 2.2 are excluded at 95% CL in the mass range of $225 < m_A < 350$ GeV.

The present analysis supersedes the previous search for the $A \to Zh$ decay carried out by the CMS Collaboration in the $(Z \to \nu\bar{\nu}/\ell\ell)(h \to b\bar{b})$ and $(Z \to \ell\ell)(h \to \tau\tau)$ channels (where $\ell = e, \mu$) [20, 22] on proton-proton collision data collected at $\sqrt{s} = 13$ TeV and corresponding to an integrated luminosity of 36 fb^{-1}.

Acknowledgments

We congratulate our colleagues in the CERN accelerator departments for the excellent performance of the LHC and thank the technical and administrative staffs at CERN and at other CMS institutes for their contributions to the success of the CMS effort. In addition, we gratefully acknowledge the computing centres and personnel of the Worldwide LHC Computing Grid and other centres for delivering so effectively the computing infrastructure essential to our analyses. Finally, we acknowledge the enduring support for the construction and operation of the LHC, the CMS detector, and the supporting computing infrastructure provided by the following funding agencies: SC (Armenia), BMBWF and FWF (Austria); FNRS and FWO (Belgium); CNPq, CAPES, FAPERJ, FAPERGS, and FAPESP (Brazil); MES and BNSF (Bulgaria); CERN; CAS, MoST, and NSFC (China); MINCIENCIAS (Colombia); MSES and CSF (Croatia); RIF (Cyprus); SENESCYT (Ecuador); ERC PRG, RVTT3 and MoER TK202 (Estonia); Academy of Finland, MEC, and HIP (Finland); CEA and CNRS/IN2P3 (France); SRNSF (Georgia); BMBF, DFG, and HGF (Germany); GSRI (Greece); NKFIH (Hungary); DAE and DST (India); IPM (Iran); SFI (Ireland); INFN (Italy); MSIP and NRF (Republic of Korea); MES (Latvia); LMTLT (Lithuania); MOE and UM (Malaysia); BUAP, CINVESTAV, CONACYT, LNS, SEP, and UASLP-FAI (Mexico); MOS (Montenegro); MBIE (New Zealand); PAEC (Pakistan); MES and NSC (Poland); FCT (Portugal); MESTD (Serbia); MCIN/AEI and PCTI (Spain); MOSTR (Sri Lanka); Swiss Funding Agencies (Switzerland); MST (Taipei); MHESI and NSTDA (Thailand); TUBITAK and TENMAK (Turkey); NASU (Ukraine); STFC (United Kingdom); DOE and NSF (USA).

Individuals have received support from the Marie-Curie programme and the European Research Council and Horizon 2020 Grant, contract Nos. 675440, 724704, 752730, 758316, 765710, 824093, 101115353, 101002207, and COST Action CA16108 (European Union); the Leventis Foundation; the Alfred P. Sloan Foundation; the Alexander von Humboldt Foundation; the Science Committee, project no. 22rl-037 (Armenia); the Fonds pour la Formation à la Recherche dans l'Industrie et dans l'Agriculture (FRIA-Belgium); the Beijing Municipal Science & Technology Commission, No. Z191100007219010 and Fundamental Research Funds for the Central Universities (China); the Ministry of Education, Youth and Sports (MEYS) of the Czech Republic; the Shota Rustaveli National Science Foundation, grant FR-22-985 (Georgia); the Deutsche Forschungsgemeinschaft (DFG), among others, under Germany's Excellence Strategy – EXC 2121 "Quantum Universe" – 390833306, and under project number 400140256 - GRK2497; the Hellenic Foundation for Research and Innovation (HFRI), Project Number 2288 (Greece); the Hungarian Academy of Sciences, the New National Excellence Program - ÚNKP, the NKFIH research grants K 131991, K 133046, K 138136, K 143460, K 143477, K 146913, K 146914, K 147048, 2020-2.2.1-ED-2021-00181, TKP2021-NKTA-64, and 2021-4.1.2-NEMZ_KI-2024-00036 (Hungary); the Council of Science and Industrial Research, India; ICSC – National Research Centre for High Performance Computing, Big Data and Quantum Computing and FAIR – Future Artificial Intelligence Research, funded by the NextGenerationEU program (Italy); the Latvian Council of Science; the Ministry of Education and Science, project no. 2022/WK/14, and the National Science Center, contracts Opus 2021/41/B/ST2/01369 and 2021/43/B/ST2/01552 (Poland); the Fundação para a Ciência e a Tecnologia, grant CEECIND/01334/2018 (Portugal); the National Priorities Research Program by Qatar National Research Fund; MCIN/AEI/10.13039/501100011033, ERDF "a way of making Europe", and the Programa Estatal de Fomento de la Investigación Científica y Técnica de Excelencia María de Maeztu, grant MDM-2017-0765 and Programa Severo Ochoa del Principado de Asturias (Spain); the Chulalongkorn Academic into Its 2nd Century Project Advancement Project, and the National Science, Research and Innovation Fund via the Program Management Unit for

Human Resources & Institutional Development, Research and Innovation, grant B39G670016 (Thailand); the Kavli Foundation; the Nvidia Corporation; the SuperMicro Corporation; the Welch Foundation, contract C-1845; and the Weston Havens Foundation (USA).

References

[1] ATLAS Collaboration, "Observation of a new particle in the search for the standard model Higgs boson with the ATLAS detector at the LHC", *Phys. Lett. B* **716** (2012) 1, doi:10.1016/j.physletb.2012.08.020, arXiv:1207.7214.

[2] CMS Collaboration, "Observation of a new boson at a mass of 125 GeV with the CMS experiment at the LHC", *Phys. Lett. B* **716** (2012) 30, doi:10.1016/j.physletb.2012.08.021, arXiv:1207.7235.

[3] CMS Collaboration, "Observation of a new boson with mass near 125 GeV in pp collisions at $\sqrt{s} = 7$ and 8 TeV", *JHEP* **06** (2013) 081, doi:10.1007/JHEP06(2013)081, arXiv:1303.4571.

[4] ATLAS Collaboration, "A detailed map of Higgs boson interactions by the ATLAS experiment ten years after the discovery", *Nature* **607** (2022) 52, doi:10.1038/s41586-022-04893-w, arXiv:2207.00092. [Erratum: doi:10.1038/s41586-022-05581-5].

[5] CMS Collaboration, "A portrait of the Higgs boson by the CMS experiment ten years after the discovery.", *Nature* **607** (2022) 60, doi:10.1038/s41586-022-04892-x, arXiv:2207.00043. [Author correction: doi:10.1038/s41586-023-06164-8].

[6] ATLAS and CMS Collaborations, "Measurements of the Higgs boson production and decay rates and constraints on its couplings from a combined ATLAS and CMS analysis of the LHC pp collision data at $\sqrt{s} = 7$ and 8 TeV", *JHEP* **08** (2016) 045, doi:10.1007/JHEP08(2016)045, arXiv:1606.02266.

[7] CMS Collaboration, "Combined measurements of Higgs boson couplings in proton–proton collisions at $\sqrt{s} = 13$ TeV", *Eur. Phys. J. C* **79** (2019) 421, doi:10.1140/epjc/s10052-019-6909-y, arXiv:1809.10733.

[8] ATLAS Collaboration, "Combined measurements of Higgs boson production and decay using up to 80 fb^{-1} of proton-proton collision data at $\sqrt{s} = 13$ TeV collected with the ATLAS experiment", *Phys. Rev. D* **101** (2020) 012002, doi:10.1103/PhysRevD.101.012002, arXiv:1909.02845.

[9] CMS Collaboration, "Measurements of the Higgs boson width and anomalous HVV couplings from on-shell and off-shell production in the four-lepton final state", *Phys. Rev. D* **99** (2019) 112003, doi:10.1103/PhysRevD.99.112003, arXiv:1901.00174.

[10] CMS Collaboration, "A measurement of the Higgs boson mass in the diphoton decay channel", *Phys. Lett. B* **805** (2020) 135425, doi:10.1016/j.physletb.2020.135425, arXiv:2002.06398.

[11] T. D. Lee, "A theory of spontaneous T violation", *Phys. Rev. D* **8** (1973) 1226, doi:10.1103/PhysRevD.8.1226.

[12] G. C. Branco et al., "Theory and phenomenology of two-Higgs-doublet models", *Phys. Rept.* **516** (2012) 1, doi:10.1016/j.physrep.2012.02.002, arXiv:1106.0034.

[13] L. Fromme, S. J. Huber, and M. Seniuch, "Baryogenesis in the two-Higgs doublet model", *JHEP* **11** (2006) 038, doi:10.1088/1126-6708/2006/11/038, arXiv:hep-ph/0605242.

[14] P. Fayet, "Supergauge invariant extension of the Higgs mechanism and a model for the electron and its neutrino", *Nucl. Phys. B* **90** (1975) 104, doi:10.1016/0550-3213(75)90636-7.

[15] P. Fayet, "Spontaneously broken supersymmetric theories of weak, electromagnetic and strong interactions", *Phys. Lett. B* **69** (1977) 489, doi:10.1016/0370-2693(77)90852-8.

[16] H. E. Haber and G. L. Kane, "The search for Supersymmetry: probing physics beyond the Standard Model", *Phys. Rept.* **117** (1985) 75, doi:10.1016/0370-1573(85)90051-1.

[17] H. Bahl, S. Liebler, and T. Stefaniak, "MSSM Higgs benchmark scenarios for Run 2 and beyond: the low tan β region", *Eur. Phys. J. C* **79** (2019) 279, doi:10.1140/epjc/s10052-019-6770-z, arXiv:1901.05933.

[18] ATLAS Collaboration, "Search for a CP-odd Higgs boson decaying to Zh in pp collisions at $\sqrt{s} = 8$ TeV with the ATLAS detector", *Phys. Lett. B* **744** (2015) 163, doi:10.1016/j.physletb.2015.03.054, arXiv:1502.04478.

[19] CMS Collaboration, "Searches for a heavy scalar boson H decaying to a pair of 125 GeV Higgs bosons hh or for a heavy pseudoscalar boson A decaying to Zh, in the final states with $h \to \tau\tau$", *Phys. Lett. B* **755** (2016) 217, doi:10.1016/j.physletb.2016.01.056, arXiv:1510.01181.

[20] CMS Collaboration, "Search for a heavy pseudoscalar Higgs boson decaying into a 125 GeV Higgs boson and a Z boson in final states with two tau and two light leptons at $\sqrt{s} = 13$ TeV", *JHEP* **03** (2020) 065, doi:10.1007/JHEP03(2020)065, arXiv:1910.11634.

[21] ATLAS Collaboration, "Search for heavy resonances decaying into a W or Z boson and a Higgs boson in final states with leptons and b-jets in 36 fb^{-1} of $\sqrt{s} = 13$ TeV pp collisions with the ATLAS detector", *JHEP* **03** (2018) 174, doi:10.1007/JHEP03(2018)174, arXiv:1712.06518. [Erratum: doi:10.1007/JHEP11(2018)051].

[22] CMS Collaboration, "Search for a heavy pseudoscalar boson decaying to a Z and a Higgs boson at $\sqrt{s} = 13$ TeV", *Eur. Phys. J. C* **79** (2019) 564, doi:10.1140/epjc/s10052-019-7058-z, arXiv:1903.00941.

[23] ATLAS Collaboration, "Search for heavy resonances decaying into a Z or W boson and a Higgs boson in final states with leptons and b-jets in 139 fb^{-1} of pp collisions at $\sqrt{s} = 13$ TeV with the ATLAS detector", *JHEP* **06** (2023) 016, doi:10.1007/JHEP06(2023)016, arXiv:2207.00230.

[24] L. Bianchini et al., "Reconstruction of the Higgs mass in events with Higgs bosons decaying into a pair of τ leptons using matrix element techniques", *Nucl. Instrum. Meth. A* **862** (2017) 54, doi:10.1016/j.nima.2017.05.001, arXiv:1603.05910.

[25] W. Matyszkiewicz and A. Kalinowski, "Tau-pair invariant mass estimation using maximum likelihood estimation and collinear approximation", *Acta Phys. Polon. Supp.* **18** (2025), no. 5, 5–A21, doi:10.5506/APhysPolBSupp.18.5-A21.

[26] CMS Collaboration, "Identification of hadronic tau lepton decays using a deep neural network", *JINST* **17** (2022) P07023, doi:10.1088/1748-0221/17/07/P07023, arXiv:2201.08458.

[27] E. Bols et al., "Jet flavour classification using DeepJet", *JINST* **15** (2020) P12012, doi:10.1088/1748-0221/15/12/P12012, arXiv:2008.10519.

[28] HEPData record for this analysis, 2025. doi:10.17182/hepdata.155628.

[29] CMS Collaboration, "Performance of the CMS Level-1 trigger in proton-proton collisions at $\sqrt{s} = 13$ TeV", *JINST* **15** (2020) P10017, doi:10.1088/1748-0221/15/10/P10017, arXiv:2006.10165.

[30] CMS Collaboration, "The CMS trigger system", *JINST* **12** (2017) P01020, doi:10.1088/1748-0221/12/01/P01020, arXiv:1609.02366.

[31] CMS Collaboration, "The CMS experiment at the CERN LHC", *JINST* **3** (2008) S08004, doi:10.1088/1748-0221/3/08/S08004.

[32] CMS Collaboration, "Particle-flow reconstruction and global event description with the CMS detector", *JINST* **12** (2017) P10003, doi:10.1088/1748-0221/12/10/P10003, arXiv:1706.04965.

[33] CMS Collaboration, "Technical proposal for the Phase-II upgrade of the Compact Muon Solenoid", CMS Technical Proposal CERN-LHCC-2015-010, CMS-TDR-15-02, 2015.

[34] CMS Collaboration, "Electron and photon reconstruction and identification with the CMS experiment at the CERN LHC", *JINST* **16** (2021) P05014, doi:10.1088/1748-0221/16/05/P05014, arXiv:2012.06888.

[35] CMS Collaboration, "Performance of the CMS muon detector and muon reconstruction with proton-proton collisions at $\sqrt{s} = 13$ TeV", *JINST* **13** (2018) P06015, doi:10.1088/1748-0221/13/06/P06015, arXiv:1804.04528.

[36] M. Cacciari, G. P. Salam, and G. Soyez, "The anti-k_{T} jet clustering algorithm", *JHEP* **04** (2008) 063, doi:10.1088/1126-6708/2008/04/063, arXiv:0802.1189.

[37] M. Cacciari, G. P. Salam, and G. Soyez, "FastJet user manual", *Eur. Phys. J. C* **72** (2012) 1896, doi:10.1140/epjc/s10052-012-1896-2, arXiv:1111.6097.

[38] CMS Collaboration, "Jet energy scale and resolution in the CMS experiment in pp collisions at 8 TeV", *JINST* **12** (2017) P02014, doi:10.1088/1748-0221/12/02/P02014, arXiv:1607.03663.

[39] CMS Collaboration, "Identification of heavy-flavour jets with the CMS detector in pp collisions at 13 TeV", *JINST* **13** (2018) P05011, doi:10.1088/1748-0221/13/05/P05011, arXiv:1712.07158.

[40] CMS Collaboration, "Performance of the DeepJet b tagging algorithm using 41.9 fb^{-1} of data from proton-proton collisions at 13 TeV with Phase 1 CMS detector", CMS Detector Performance Summary CMS-DP-2020-021, 2018.

[41] CMS Collaboration, "Performance of reconstruction and identification of τ leptons decaying to hadrons and ν_τ in pp collisions at $\sqrt{s} = 13$ TeV", *JINST* **13** (2018) P10005, doi:10.1088/1748-0221/13/10/P10005, arXiv:1809.02816.

[42] CMS Collaboration, "Performance of missing transverse momentum reconstruction in proton-proton collisions at $\sqrt{s} = 13$ TeV using the CMS detector", *JINST* **14** (2019) P07004, doi:10.1088/1748-0221/14/07/P07004, arXiv:1903.06078.

[43] J. Alwall et al., "The automated computation of tree-level and next-to-leading order differential cross sections, and their matching to parton shower simulations", *JHEP* **07** (2014) 079, doi:10.1007/JHEP07(2014)079, arXiv:1405.0301.

[44] P. Artoisenet, R. Frederix, O. Mattelaer, and R. Rietkerk, "Automatic spin-entangled decays of heavy resonances in Monte Carlo simulations", *JHEP* **03** (2013) 015, doi:10.1007/JHEP03(2013)015, arXiv:1212.3460.

[45] J. Alwall et al., "Comparative study of various algorithms for the merging of parton showers and matrix elements in hadronic collisions", *Eur. Phys. J. C* **53** (2008) 473, doi:10.1140/epjc/s10052-007-0490-5, arXiv:0706.2569.

[46] S. P. Martin, "A Supersymmetry primer", *Adv. Ser. Direct. HEP* **21** (2010) 1, doi:10.1142/9789814307505_0001, arXiv:hep-ph/9709356.

[47] P. Nason, "A new method for combining NLO QCD with shower Monte Carlo algorithms", *JHEP* **11** (2004) 040, doi:10.1088/1126-6708/2004/11/040, arXiv:hep-ph/0409146.

[48] S. Frixione, P. Nason, and C. Oleari, "Matching NLO QCD computations with parton shower simulations: the POWHEG method", *JHEP* **11** (2007) 070, doi:10.1088/1126-6708/2007/11/070, arXiv:0709.2092.

[49] S. Alioli, P. Nason, C. Oleari, and E. Re, "A general framework for implementing NLO calculations in shower Monte Carlo programs: the POWHEG BOX", *JHEP* **06** (2010) 043, doi:10.1007/JHEP06(2010)043, arXiv:1002.2581.

[50] G. Luisoni, P. Nason, C. Oleari, and F. Tramontano, "$HW^{\pm}/HZ$ + 0 and 1 jet at NLO with the POWHEG BOX interfaced to GoSam and their merging within MiNLO", *JHEP* **10** (2013) 083, doi:10.1007/JHEP10(2013)083, arXiv:1306.2542.

[51] F. Granata, J. M. Lindert, C. Oleari, and S. Pozzorini, "NLO QCD+EW predictions for HV and HV+jet production including parton-shower effects", *JHEP* **09** (2017) 012, doi:10.1007/JHEP09(2017)012, arXiv:1706.03522.

[52] H. B. Hartanto, B. Jager, L. Reina, and D. Wackeroth, "Higgs boson production in association with top quarks in the POWHEG BOX", *Phys. Rev. D* **91** (2015) 094003, doi:10.1103/PhysRevD.91.094003, arXiv:1501.04498.

[53] S. Bolognesi et al., "On the spin and parity of a single-produced resonance at the LHC", *Phys. Rev. D* **86** (2012) 095031, doi:10.1103/PhysRevD.86.095031, arXiv:1208.4018.

[54] LHC Higgs Cross Section Working Group, "Handbook of LHC Higgs cross sections: 4. Deciphering the nature of the Higgs sector", CERN Report CERN-2017-002-M, 2016. doi:10.23731/CYRM-2017-002, arXiv:1610.07922.

[55] J. M. Campbell, R. K. Ellis, and C. Williams, "Vector boson pair production at the LHC", *JHEP* **07** (2011) 018, doi:10.1007/JHEP07(2011)018, arXiv:1105.0020.

[56] P. Nason and G. Zanderighi, "W^+W^- , WZ and ZZ production in the POWHEG-BOX-V2", *Eur. Phys. J. C* **74** (2014) 2702, doi:10.1140/epjc/s10052-013-2702-5, arXiv:1311.1365.

[57] R. Frederix and S. Frixione, "Merging meets matching in MC@NLO", *JHEP* **12** (2012) 061, doi:10.1007/JHEP12(2012)061, arXiv:1209.6215.

[58] S. Alioli, S.-O. Moch, and P. Uwer, "Hadronic top-quark pair-production with one jet and parton showering", *JHEP* **01** (2012) 137, doi:10.1007/JHEP01(2012)137, arXiv:1110.5251.

[59] F. Caola et al., "QCD corrections to vector boson pair production in gluon fusion including interference effects with off-shell Higgs at the LHC", *JHEP* **07** (2016) 087, doi:10.1007/JHEP07(2016)087, arXiv:1605.04610.

[60] T. Gehrmann et al., "W^+W^- production at hadron colliders in next to next to leading order QCD", *Phys. Rev. Lett.* **113** (2014) 212001, doi:10.1103/PhysRevLett.113.212001, arXiv:1408.5243.

[61] K. Melnikov and F. Petriello, "Electroweak gauge boson production at hadron colliders through $\mathcal{O}(\alpha_s^2)$", *Phys. Rev. D* **74** (2006) 114017, doi:10.1103/PhysRevD.74.114017, arXiv:hep-ph/0609070.

[62] M. Czakon and A. Mitov, "Top++: A program for the calculation of the top-pair cross-section at hadron colliders", *Comput. Phys. Commun.* **185** (2014) 2930, doi:10.1016/j.cpc.2014.06.021, arXiv:1112.5675.

[63] J. M. Campbell and R. K. Ellis, "$t\bar{t}W^{\pm}$ production and decay at NLO", *JHEP* **07** (2012) 052, doi:10.1007/JHEP07(2012)052, arXiv:1204.5678.

[64] M. V. Garzelli, A. Kardos, C. G. Papadopoulos, and Z. Trocsanyi, "$t\bar{t}W^{\pm}$ and $t\bar{t}Z$ hadroproduction at NLO accuracy in QCD with parton shower and hadronization effects", *JHEP* **11** (2012) 056, doi:10.1007/JHEP11(2012)056, arXiv:1208.2665.

[65] NNPDF Collaboration, "Parton distributions from high-precision collider data", *Eur. Phys. J. C* **77** (2017) 663, doi:10.1140/epjc/s10052-017-5199-5, arXiv:1706.00428.

[66] T. Sjöstrand et al., "An introduction to PYTHIA 8.2", *Comput. Phys. Commun.* **191** (2015) 159, doi:10.1016/j.cpc.2015.01.024, arXiv:1410.3012.

[67] CMS Collaboration, "Extraction and validation of a new set of CMS PYTHIA8 tunes from underlying-event measurements", *Eur. Phys. J. C* **80** (2020) 4, doi:10.1140/epjc/s10052-019-7499-4, arXiv:1903.12179.

[68] GEANT4 Collaboration, "GEANT4—a simulation toolkit", *Nucl. Instrum. Meth. A* **506** (2003) 250, doi:10.1016/S0168-9002(03)01368-8.

[69] R. D. Cousins, "Lectures on statistics in theory: Prelude to statistics in practice", 2018. arXiv:1807.05996.

[70] CMS Collaboration, "The CMS statistical analysis and combination tool: COMBINE", *Comput. Softw. Big Sci.* **8** (2024) 19, doi:10.1007/s41781-024-00121-4, arXiv:2404.06614.

[71] J. Butterworth et al., "PDF4LHC recommendations for LHC Run II", *J. Phys. G* **43** (2016) 023001, doi:10.1088/0954-3899/43/2/023001, arXiv:1510.03865.

[72] CMS Collaboration, "Measurement of the cross section for top quark pair production in association with a W or Z boson in proton-proton collisions at $\sqrt{s} = 13$ TeV", *JHEP* **08** (2018) 011, doi:10.1007/JHEP08(2018)011, arXiv:1711.02547.

[73] E. A. Bagnaschi et al., "Benchmark scenarios for MSSM Higgs boson searches at the LHC", CERN Report LHCHWG-2021-001, 2021.

[74] CMS Collaboration, "Precision luminosity measurement in proton-proton collisions at $\sqrt{s} = 13$ TeV in 2015 and 2016 at CMS", *Eur. Phys. J. C* **81** (2021) 800, doi:10.1140/epjc/s10052-021-09538-2, arXiv:2104.01927.

[75] CMS Collaboration, "CMS luminosity measurement for the 2017 data-taking period at $\sqrt{s}$ = 13 TeV", CMS Physics Analysis Summary CMS-PAS-LUM-17-004, 2018.

[76] CMS Collaboration, "CMS luminosity measurement for the 2018 data-taking period at $\sqrt{s}$ = 13 TeV", CMS Physics Analysis Summary CMS-PAS-LUM-18-002, 2019.

[77] R. J. Barlow and C. Beeston, "Fitting using finite Monte Carlo samples", *Comput. Phys. Commun.* **77** (1993) 219, doi:10.1016/0010-4655(93)90005-W.

[78] J. S. Conway, "Incorporating nuisance parameters in likelihoods for multisource spectra", in *PHYSTAT 2011*, p. 115. 2011. arXiv:1103.0354. doi:10.5170/CERN-2011-006.115.

[79] W. Verkerke and D. P. Kirkby, "The RooFit toolkit for data modeling", in *Proc. PHYSTAT 2003, Statistical Problems in Particle Physics, Astrophysics and Cosmology*, L. Lyons and M. Karagoz, eds., p. MOLT007. 2003. arXiv:physics/0306116. eConf C0303241.

[80] L. Moneta et al., "The RooStats project", in *Proc. ACAT 2010, 13th International Workshop on Advanced Computing and Analysis Techniques in Physics Research*, p. 057. 2010. arXiv:1009.1003. PoS ACAT2010. doi:10.22323/1.093.0057.

[81] CMS Collaboration, "Combined results of searches for the standard model Higgs boson in pp collisions at $\sqrt{s} = 7$ TeV", *Phys. Lett. B* **710** (2012) 26, doi:10.1016/j.physletb.2012.02.064, arXiv:1202.1488.

[82] T. Junk, "Confidence level computation for combining searches with small statistics", *Nucl. Instrum. Meth. A* **434** (1999) 435, doi:10.1016/S0168-9002(99)00498-2, arXiv:hep-ex/9902006.

[83] A. L. Read, "Presentation of search results: The CL_s technique", *J. Phys. G* **28** (2002) 2693, doi:10.1088/0954-3899/28/10/313.

[84] S. Heinemeyer, W. Hollik, and G. Weiglein, "FeynHiggs: A program for the calculation of the masses of the neutral CP-even Higgs bosons in the MSSM", *Comput. Phys. Commun.* **124** (2000) 76, doi:10.1016/S0010-4655(99)00364-1, arXiv:hep-ph/9812320.

[85] S. Heinemeyer, W. Hollik, and G. Weiglein, "The masses of the neutral CP-even Higgs bosons in the MSSM: Accurate analysis at the two-loop level", *Eur. Phys. J. C* **9** (1999) 343, doi:10.1007/s100529900006, arXiv:hep-ph/9812472.

[86] G. Degrassi et al., "Towards high-precision predictions for the MSSM Higgs sector", *Eur. Phys. J. C* **28** (2003) 133, doi:10.1140/epjc/s2003-01152-2, arXiv:hep-ph/0212020.

[87] M. Frank et al., "The Higgs boson masses and mixings of the complex MSSM in the Feynman-diagrammatic approach", *JHEP* **02** (2007) 047, doi:10.1088/1126-6708/2007/02/047, arXiv:hep-ph/0611326.

[88] T. Hahn et al., "High-precision predictions for the light CP-even Higgs boson mass of the minimal supersymmetric standard model", *Phys. Rev. Lett.* **112** (2014) 141801, doi:10.1103/PhysRevLett.112.141801, arXiv:1312.4937.

[89] H. Bahl and W. Hollik, "Precise prediction for the light MSSM Higgs boson mass combining effective field theory and fixed-order calculations", *Eur. Phys. J. C* **76** (2016) 499, doi:10.1140/epjc/s10052-016-4354-8, arXiv:1608.01880.

[90] H. Bahl, S. Heinemeyer, W. Hollik, and G. Weiglein, "Reconciling EFT and hybrid calculations of the light MSSM Higgs-boson mass", *Eur. Phys. J. C* **78** (2018) 57, doi:10.1140/epjc/s10052-018-5544-3, arXiv:1706.00346.

[91] H. Bahl et al., "Precision calculations in the MSSM Higgs-boson sector with FeynHiggs 2.14", *Comput. Phys. Commun.* **249** (2020) 107099, doi:10.1016/j.cpc.2019.107099, arXiv:1811.09073.

[92] A. Djouadi, J. Kalinowski, M. Muehlleitner, and M. Spira, "HDECAY: Twenty++ years after", *Comput. Phys. Commun.* **238** (2019) 214, doi:10.1016/j.cpc.2018.12.010, arXiv:1801.09506.

[93] LHC Higgs Cross Section Working Group, "Handbook of LHC Higgs cross sections: 3. Higgs properties", CERN Report CERN-2013-004, 2013. doi:10.5170/CERN-2013-004, arXiv:1307.1347.

[94] A. Denner et al., "Standard model Higgs-boson branching ratios with uncertainties", *Eur. Phys. J. C* **71** (2011) 1753, doi:10.1140/epjc/s10052-011-1753-8, arXiv:1107.5909.

[95] R. V. Harlander, S. Liebler, and H. Mantler, "SusHi: A program for the calculation of Higgs production in gluon fusion and bottom-quark annihilation in the standard model and the MSSM", *Comput. Phys. Commun.* **184** (2013) 1605, doi:10.1016/j.cpc.2013.02.006, arXiv:1212.3249.

[96] R. V. Harlander, S. Liebler, and H. Mantler, "SusHi Bento: Beyond NNLO and the heavy-top limit", *Comput. Phys. Commun.* **212** (2017) 239, doi:10.1016/j.cpc.2016.10.015, arXiv:1605.03190.

[97] M. Spira, A. Djouadi, D. Graudenz, and P. M. Zerwas, "Higgs boson production at the LHC", *Nucl. Phys. B* **453** (1995) 17, doi:10.1016/0550-3213(95)00379-7, arXiv:hep-ph/9504378.

[98] R. Harlander and P. Kant, "Higgs production and decay: analytic results at next-to-leading order QCD", *JHEP* **12** (2005) 015, doi:10.1088/1126-6708/2005/12/015, arXiv:hep-ph/0509189.

[99] R. V. Harlander and W. B. Kilgore, "Next-to-next-to-leading order Higgs production at hadron colliders", *Phys. Rev. Lett.* **88** (2002) 201801, doi:10.1103/PhysRevLett.88.201801, arXiv:hep-ph/0201206.

[100] C. Anastasiou and K. Melnikov, "Higgs boson production at hadron colliders in NNLO QCD", *Nucl. Phys. B* **646** (2002) 220, doi:10.1016/S0550-3213(02)00837-4, arXiv:hep-ph/0207004.

[101] V. Ravindran, J. Smith, and W. L. van Neerven, "NNLO corrections to the total cross-section for Higgs boson production in hadron-hadron collisions", *Nucl. Phys. B* **665** (2003) 325, doi:10.1016/S0550-3213(03)00457-7, arXiv:hep-ph/0302135.

[102] R. V. Harlander and W. B. Kilgore, "Production of a pseudo-scalar Higgs boson at hadron colliders at next-to-next-to leading order", *JHEP* **10** (2002) 017, doi:10.1088/1126-6708/2002/10/017, arXiv:hep-ph/0208096.

[103] C. Anastasiou and K. Melnikov, "Pseudoscalar Higgs boson production at hadron colliders in next-to-next-to-leading order QCD", *Phys. Rev. D* **67** (2003) 037501, doi:10.1103/PhysRevD.67.037501, arXiv:hep-ph/0208115.

[104] C. Anastasiou et al., "Higgs boson gluon-fusion production beyond threshold in N^3LO QCD", *JHEP* **03** (2015) 091, doi:10.1007/JHEP03(2015)091, arXiv:1411.3584.

[105] C. Anastasiou et al., "Soft expansion of double-real-virtual corrections to Higgs production at N^3LO", *JHEP* **08** (2015) 051, doi:10.1007/JHEP08(2015)051, arXiv:1505.04110.

[106] C. Anastasiou et al., "High precision determination of the gluon fusion Higgs boson cross-section at the LHC", *JHEP* **05** (2016) 058, doi:10.1007/JHEP05(2016)058, arXiv:1602.00695.

[107] U. Aglietti, R. Bonciani, G. Degrassi, and A. Vicini, "Two-loop light fermion contribution to Higgs production and decays", *Phys. Lett. B* **595** (2004) 432, doi:10.1016/j.physletb.2004.06.063, arXiv:hep-ph/0404071.

[108] R. Bonciani, G. Degrassi, and A. Vicini, "On the generalized harmonic polylogarithms of one complex variable", *Comput. Phys. Commun.* **182** (2011) 1253, doi:10.1016/j.cpc.2011.02.011, arXiv:1007.1891.

[109] M. Bonvini, A. S. Papanastasiou, and F. J. Tackmann, "Resummation and matching of b-quark mass effects in $b\bar{b}H$ production", *JHEP* **11** (2015) 196, doi:10.1007/JHEP11(2015)196, arXiv:1508.03288.

[110] M. Bonvini, A. S. Papanastasiou, and F. J. Tackmann, "Matched predictions for the $b\bar{b}H$ cross section at the 13 TeV LHC", *JHEP* **10** (2016) 053, doi:10.1007/JHEP10(2016)053, arXiv:1605.01733.

[111] S. Forte, D. Napoletano, and M. Ubiali, "Higgs production in bottom-quark fusion in a matched scheme", *Phys. Lett. B* **751** (2015) 331, doi:10.1016/j.physletb.2015.10.051, arXiv:1508.01529.

[112] S. Forte, D. Napoletano, and M. Ubiali, "Higgs production in bottom-quark fusion: matching beyond leading order", *Phys. Lett. B* **763** (2016) 190, doi:10.1016/j.physletb.2016.10.040, arXiv:1607.00389.

[113] R. V. Harlander and W. B. Kilgore, "Higgs boson production in bottom quark fusion at next-to-next-to leading order", *Phys. Rev. D* **68** (2003) 013001, doi:10.1103/PhysRevD.68.013001, arXiv:hep-ph/0304035.

[114] S. Dittmaier, M. Krämer, and M. Spira, "Higgs radiation off bottom quarks at the Fermilab Tevatron and the CERN LHC", *Phys. Rev. D* **70** (2004) 074010, doi:10.1103/PhysRevD.70.074010, arXiv:hep-ph/0309204.

[115] S. Dawson, C. B. Jackson, L. Reina, and D. Wackeroth, "Exclusive Higgs boson production with bottom quarks at hadron colliders", *Phys. Rev. D* **69** (2004) 074027, doi:10.1103/PhysRevD.69.074027, arXiv:hep-ph/0311067.

A The CMS Collaboration

Yerevan Physics Institute, Yerevan, Armenia
V. Chekhovsky, A. Hayrapetyan, V. Makarenko, A. Tumasyan[1]

Institut für Hochenergiephysik, Vienna, Austria
W. Adam, J.W. Andrejkovic, L. Benato, T. Bergauer, S. Chatterjee, K. Damanakis, M. Dragicevic, P.S. Hussain, M. Jeitler[2], N. Krammer, A. Li, D. Liko, I. Mikulec, J. Schieck[2], R. Schöfbeck[2], D. Schwarz, M. Sonawane, W. Waltenberger, C.-E. Wulz[2]

Universiteit Antwerpen, Antwerpen, Belgium
T. Janssen, H. Kwon, T. Van Laer, P. Van Mechelen

Vrije Universiteit Brussel, Brussel, Belgium
N. Breugelmans, J. D'Hondt, S. Dansana, A. De Moor, M. Delcourt, F. Heyen, Y. Hong, S. Lowette, I. Makarenko, D. Müller, S. Tavernier, M. Tytgat[3], G.P. Van Onsem, S. Van Putte, D. Vannerom

Université Libre de Bruxelles, Bruxelles, Belgium
B. Bilin, B. Clerbaux, A.K. Das, I. De Bruyn, G. De Lentdecker, H. Evard, L. Favart, P. Gianneios, A. Khalilzadeh, F.A. Khan, K. Lee, A. Malara, M.A. Shahzad, L. Thomas, M. Vanden Bemden, C. Vander Velde, P. Vanlaer

Ghent University, Ghent, Belgium
M. De Coen, D. Dobur, G. Gokbulut, J. Knolle, L. Lambrecht, D. Marckx, K. Mota Amarilo, K. Skovpen, N. Van Den Bossche, J. van der Linden, L. Wezenbeek

Université Catholique de Louvain, Louvain-la-Neuve, Belgium
S. Bein, A. Benecke, A. Bethani, G. Bruno, C. Caputo, J. De Favereau De Jeneret, C. Delaere, I.S. Donertas, A. Giammanco, A.O. Guzel, Sa. Jain, V. Lemaitre, J. Lidrych, P. Mastrapasqua, T.T. Tran, S. Turkcapar

Centro Brasileiro de Pesquisas Fisicas, Rio de Janeiro, Brazil
G.A. Alves, E. Coelho, G. Correia Silva, C. Hensel, T. Menezes De Oliveira, C. Mora Herrera[4], P. Rebello Teles, M. Soeiro, E.J. Tonelli Manganote[5], A. Vilela Pereira[4]

Universidade do Estado do Rio de Janeiro, Rio de Janeiro, Brazil
W.L. Aldá Júnior, M. Barroso Ferreira Filho, H. Brandao Malbouisson, W. Carvalho, J. Chinellato[6], E.M. Da Costa, G.G. Da Silveira[7], D. De Jesus Damiao, S. Fonseca De Souza, R. Gomes De Souza, T. Laux Kuhn[7], M. Macedo, J. Martins, L. Mundim, H. Nogima, J.P. Pinheiro, A. Santoro, A. Sznajder, M. Thiel

Universidade Estadual Paulista, Universidade Federal do ABC, São Paulo, Brazil
C.A. Bernardes[7], L. Calligaris, T.R. Fernandez Perez Tomei, E.M. Gregores, I. Maietto Silverio, P.G. Mercadante, S.F. Novaes, B. Orzari, Sandra S. Padula

Institute for Nuclear Research and Nuclear Energy, Bulgarian Academy of Sciences, Sofia, Bulgaria
A. Aleksandrov, G. Antchev, R. Hadjiiska, P. Iaydjiev, M. Misheva, M. Shopova, G. Sultanov

University of Sofia, Sofia, Bulgaria

A. Dimitrov, L. Litov, B. Pavlov, P. Petkov, A. Petrov, E. Shumka

Instituto De Alta Investigación, Universidad de Tarapacá, Casilla 7 D, Arica, Chile
S. Keshri, D. Laroze, S. Thakur

Beihang University, Beijing, China
T. Cheng, T. Javaid, L. Yuan

Department of Physics, Tsinghua University, Beijing, China
Z. Hu, Z. Liang, J. Liu

Institute of High Energy Physics, Beijing, China
G.M. Chen[8], H.S. Chen[8], M. Chen[8], F. Iemmi[9], C.H. Jiang, A. Kapoor[9], H. Liao, Z.-A. Liu[10], R. Sharma[11], J.N. Song[10], J. Tao, C. Wang[11], J. Wang, Z. Wang[11], H. Zhang, J. Zhao

State Key Laboratory of Nuclear Physics and Technology, Peking University, Beijing, China
A. Agapitos, Y. Ban, A. Carvalho Antunes De Oliveira, S. Deng, B. Guo, C. Jiang, A. Levin, C. Li, Q. Li, Y. Mao, S. Qian, S.J. Qian, X. Qin, X. Sun, D. Wang, H. Yang, Y. Zhao, C. Zhou

Guangdong Provincial Key Laboratory of Nuclear Science and Guangdong-Hong Kong Joint Laboratory of Quantum Matter, South China Normal University, Guangzhou, China
S. Yang

Sun Yat-Sen University, Guangzhou, China
Z. You

University of Science and Technology of China, Hefei, China
K. Jaffel, N. Lu

Nanjing Normal University, Nanjing, China
G. Bauer[12], B. Li[13], H. Wang, K. Yi[14], J. Zhang

Institute of Modern Physics and Key Laboratory of Nuclear Physics and Ion-beam Application (MOE) - Fudan University, Shanghai, China
Y. Li

Zhejiang University, Hangzhou, Zhejiang, China
Z. Lin, C. Lu, M. Xiao

Universidad de Los Andes, Bogota, Colombia
C. Avila, D.A. Barbosa Trujillo, A. Cabrera, C. Florez, J. Fraga, J.A. Reyes Vega

Universidad de Antioquia, Medellin, Colombia
J. Jaramillo, C. Rendón, M. Rodriguez, A.A. Ruales Barbosa, J.D. Ruiz Alvarez

University of Split, Faculty of Electrical Engineering, Mechanical Engineering and Naval Architecture, Split, Croatia
D. Giljanovic, N. Godinovic, D. Lelas, A. Sculac

University of Split, Faculty of Science, Split, Croatia
M. Kovac, A. Petkovic, T. Sculac

Institute Rudjer Boskovic, Zagreb, Croatia
P. Bargassa, V. Brigljevic, B.K. Chitroda, D. Ferencek, K. Jakovcic, A. Starodumov[15], T. Susa

University of Cyprus, Nicosia, Cyprus
A. Attikis, K. Christoforou, A. Hadjiagapiou, C. Leonidou, J. Mousa, C. Nicolaou, L. Paizanos, F. Ptochos, P.A. Razis, H. Rykaczewski, H. Saka, A. Stepennov

Charles University, Prague, Czech Republic
M. Finger, M. Finger Jr., A. Kveton

Escuela Politecnica Nacional, Quito, Ecuador
E. Ayala

Universidad San Francisco de Quito, Quito, Ecuador
E. Carrera Jarrin

Academy of Scientific Research and Technology of the Arab Republic of Egypt, Egyptian Network of High Energy Physics, Cairo, Egypt
A.A. Abdelalim[16,17], S. Elgammal[18], A. Ellithi Kamel[19]

Center for High Energy Physics (CHEP-FU), Fayoum University, El-Fayoum, Egypt
M. Abdullah Al-Mashad, M.A. Mahmoud

National Institute of Chemical Physics and Biophysics, Tallinn, Estonia
K. Ehataht, M. Kadastik, T. Lange, C. Nielsen, J. Pata, M. Raidal, L. Tani, C. Veelken

Department of Physics, University of Helsinki, Helsinki, Finland
K. Osterberg, M. Voutilainen

Helsinki Institute of Physics, Helsinki, Finland
N. Bin Norjoharuddeen, E. Brücken, F. Garcia, P. Inkaew, K.T.S. Kallonen, T. Lampén, K. Lassila-Perini, S. Lehti, T. Lindén, M. Myllymäki, M.m. Rantanen, J. Tuominiemi

Lappeenranta-Lahti University of Technology, Lappeenranta, Finland
H. Kirschenmann, P. Luukka, H. Petrow

IRFU, CEA, Université Paris-Saclay, Gif-sur-Yvette, France
M. Besancon, F. Couderc, M. Dejardin, D. Denegri, J.L. Faure, F. Ferri, S. Ganjour, P. Gras, G. Hamel de Monchenault, M. Kumar, V. Lohezic, J. Malcles, F. Orlandi, L. Portales, A. Rosowsky, M.Ö. Sahin, A. Savoy-Navarro[20], P. Simkina, M. Titov, M. Tornago

Laboratoire Leprince-Ringuet, CNRS/IN2P3, Ecole Polytechnique, Institut Polytechnique de Paris, Palaiseau, France
F. Beaudette, G. Boldrini, P. Busson, A. Cappati, C. Charlot, M. Chiusi, T.D. Cuisset, F. Damas, O. Davignon, A. De Wit, I.T. Ehle, B.A. Fontana Santos Alves, S. Ghosh, A. Gilbert, R. Granier de Cassagnac, A. Hakimi, B. Harikrishnan, L. Kalipoliti, G. Liu, M. Nguyen, C. Ochando, R. Salerno, J.B. Sauvan, Y. Sirois, G. Sokmen, L. Urda Gómez, E. Vernazza, A. Zabi, A. Zghiche

Université de Strasbourg, CNRS, IPHC UMR 7178, Strasbourg, France
J.-L. Agram[21], J. Andrea, D. Apparu, D. Bloch, J.-M. Brom, E.C. Chabert, C. Collard, S. Falke, U. Goerlach, R. Haeberle, A.-C. Le Bihan, M. Meena, O. Poncet, G. Saha, M.A. Sessini, P. Van Hove, P. Vaucelle

Centre de Calcul de l'Institut National de Physique Nucleaire et de Physique des Particules, CNRS/IN2P3, Villeurbanne, France

A. Di Florio

Institut de Physique des 2 Infinis de Lyon (IP2I), Villeurbanne, France
D. Amram, S. Beauceron, B. Blancon, G. Boudoul, N. Chanon, D. Contardo, P. Depasse, C. Dozen[22], H. El Mamouni, J. Fay, S. Gascon, M. Gouzevitch, C. Greenberg, G. Grenier, B. Ille, E. Jourd'huy, I.B. Laktineh, M. Lethuillier, L. Mirabito, S. Perries, A. Purohit, M. Vander Donckt, P. Verdier, J. Xiao

Georgian Technical University, Tbilisi, Georgia
D. Chokheli, I. Lomidze, Z. Tsamalaidze[23]

RWTH Aachen University, I. Physikalisches Institut, Aachen, Germany
V. Botta, S. Consuegra Rodríguez, L. Feld, K. Klein, M. Lipinski, D. Meuser, A. Pauls, D. Pérez Adán, N. Röwert, M. Teroerde

RWTH Aachen University, III. Physikalisches Institut A, Aachen, Germany
S. Diekmann, A. Dodonova, N. Eich, D. Eliseev, F. Engelke, J. Erdmann, M. Erdmann, P. Fackeldey, B. Fischer, T. Hebbeker, K. Hoepfner, F. Ivone, A. Jung, M.y. Lee, F. Mausolf, M. Merschmeyer, A. Meyer, S. Mukherjee, D. Noll, F. Nowotny, A. Pozdnyakov, Y. Rath, W. Redjeb, F. Rehm, H. Reithler, V. Sarkisovi, A. Schmidt, C. Seth, A. Sharma, J.L. Spah, F. Torres Da Silva De Araujo[24], S. Wiedenbeck, S. Zaleski

RWTH Aachen University, III. Physikalisches Institut B, Aachen, Germany
C. Dziwok, G. Flügge, T. Kress, A. Nowack, O. Pooth, A. Stahl, T. Ziemons, A. Zotz

Deutsches Elektronen-Synchrotron, Hamburg, Germany
H. Aarup Petersen, M. Aldaya Martin, J. Alimena, S. Amoroso, Y. An, J. Bach, S. Baxter, M. Bayatmakou, H. Becerril Gonzalez, O. Behnke, A. Belvedere, F. Blekman[25], K. Borras[26], A. Campbell, A. Cardini, F. Colombina, M. De Silva, G. Eckerlin, D. Eckstein, L.I. Estevez Banos, E. Gallo[25], A. Geiser, V. Guglielmi, M. Guthoff, A. Hinzmann, L. Jeppe, B. Kaech, M. Kasemann, C. Kleinwort, R. Kogler, M. Komm, D. Krücker, W. Lange, D. Leyva Pernia, K. Lipka[27], W. Lohmann[28], F. Lorkowski, R. Mankel, I.-A. Melzer-Pellmann, M. Mendizabal Morentin, A.B. Meyer, G. Milella, K. Moral Figueroa, A. Mussgiller, L.P. Nair, J. Niedziela, A. Nürnberg, J. Park, E. Ranken, A. Raspereza, D. Rastorguev, J. Rübenach, L. Rygaard, M. Scham[29,26], S. Schnake[26], P. Schütze, C. Schwanenberger[25], D. Selivanova, K. Sharko, M. Shchedrolosiev, D. Stafford, F. Vazzoler, A. Ventura Barroso, R. Walsh, D. Wang, Q. Wang, K. Wichmann, L. Wiens[26], C. Wissing, Y. Yang, S. Zakharov, A. Zimermmane Castro Santos

University of Hamburg, Hamburg, Germany
A. Albrecht, S. Albrecht, M. Antonello, S. Bollweg, M. Bonanomi, P. Connor, K. El Morabit, Y. Fischer, E. Garutti, A. Grohsjean, J. Haller, D. Hundhausen, H.R. Jabusch, G. Kasieczka, P. Keicher, R. Klanner, W. Korcari, T. Kramer, C.c. Kuo, V. Kutzner, F. Labe, J. Lange, A. Lobanov, C. Matthies, L. Moureaux, M. Mrowietz, A. Nigamova, Y. Nissan, A. Paasch, K.J. Pena Rodriguez, T. Quadfasel, B. Raciti, M. Rieger, D. Savoiu, J. Schindler, P. Schleper, M. Schröder, J. Schwandt, M. Sommerhalder, H. Stadie, G. Steinbrück, A. Tews, B. Wiederspan, M. Wolf

Karlsruher Institut fuer Technologie, Karlsruhe, Germany

S. Brommer, E. Butz, T. Chwalek, A. Dierlamm, G.G. Dincer, U. Elicabuk, N. Faltermann, M. Giffels, A. Gottmann, F. Hartmann[30], R. Hofsaess, M. Horzela, U. Husemann, J. Kieseler, M. Klute, O. Lavoryk, J.M. Lawhorn, M. Link, A. Lintuluoto, S. Maier, S. Mitra, M. Mormile, Th. Müller, M. Neukum, M. Oh, E. Pfeffer, M. Presilla, G. Quast, K. Rabbertz, B. Regnery, N. Shadskiy, I. Shvetsov, H.J. Simonis, L. Sowa, L. Stockmeier, K. Tauqeer, M. Toms, B. Topko, N. Trevisani, R.F. Von Cube, M. Wassmer, S. Wieland, F. Wittig, R. Wolf, X. Zuo

Institute of Nuclear and Particle Physics (INPP), NCSR Demokritos, Aghia Paraskevi, Greece
G. Anagnostou, G. Daskalakis, A. Kyriakis, A. Papadopoulos[30], A. Stakia

National and Kapodistrian University of Athens, Athens, Greece
G. Melachroinos, Z. Painesis, I. Paraskevas, N. Saoulidou, K. Theofilatos, E. Tziaferi, K. Vellidis, I. Zisopoulos

National Technical University of Athens, Athens, Greece
G. Bakas, T. Chatzistavrou, G. Karapostoli, K. Kousouris, I. Papakrivopoulos, E. Siamarkou, G. Tsipolitis, A. Zacharopoulou

University of Ioánnina, Ioánnina, Greece
I. Bestintzanos, I. Evangelou, C. Foudas, C. Kamtsikis, P. Katsoulis, P. Kokkas, P.G. Kosmoglou Kioseoglou, N. Manthos, I. Papadopoulos, J. Strologas

HUN-REN Wigner Research Centre for Physics, Budapest, Hungary
C. Hajdu, D. Horvath[31,32], K. Márton, A.J. Rádl[33], F. Sikler, V. Veszpremi

MTA-ELTE Lendület CMS Particle and Nuclear Physics Group, Eötvös Loránd University, Budapest, Hungary
M. Csanád, K. Farkas, A. Fehérkuti[34], M.M.A. Gadallah[35], Á. Kadlecsik, P. Major, G. Pásztor, G.I. Veres

Faculty of Informatics, University of Debrecen, Debrecen, Hungary
B. Ujvari, G. Zilizi

HUN-REN ATOMKI - Institute of Nuclear Research, Debrecen, Hungary
G. Bencze, S. Czellar, J. Molnar, Z. Szillasi

Karoly Robert Campus, MATE Institute of Technology, Gyongyos, Hungary
T. Csorgo[34], F. Nemes[34], T. Novak

Panjab University, Chandigarh, India
S. Bansal, S.B. Beri, V. Bhatnagar, G. Chaudhary, S. Chauhan, N. Dhingra[36], A. Kaur, A. Kaur, H. Kaur, M. Kaur, S. Kumar, T. Sheokand, J.B. Singh, A. Singla

University of Delhi, Delhi, India
A. Bhardwaj, A. Chhetri, B.C. Choudhary, A. Kumar, A. Kumar, M. Naimuddin, K. Ranjan, M.K. Saini, S. Saumya

Saha Institute of Nuclear Physics, HBNI, Kolkata, India
S. Baradia, S. Barman[37], S. Bhattacharya, S. Das Gupta, S. Dutta, S. Dutta, S. Sarkar

Indian Institute of Technology Madras, Madras, India
M.M. Ameen, P.K. Behera, S.C. Behera, S. Chatterjee, G. Dash, P. Jana, P. Kalbhor, S. Kamble, J.R. Komaragiri[38], D. Kumar[38], T. Mishra, B. Parida[39],

P.R. Pujahari, N.R. Saha, A. Sharma, A.K. Sikdar, R.K. Singh, P. Verma, S. Verma, A. Vijay

Tata Institute of Fundamental Research-A, Mumbai, India
S. Dugad, G.B. Mohanty, M. Shelake, P. Suryadevara

Tata Institute of Fundamental Research-B, Mumbai, India
A. Bala, S. Banerjee, S. Bhowmik, R.M. Chatterjee, M. Guchait, Sh. Jain, A. Jaiswal, B.M. Joshi, S. Kumar, G. Majumder, K. Mazumdar, S. Parolia, A. Thachayath

National Institute of Science Education and Research, An OCC of Homi Bhabha National Institute, Bhubaneswar, Odisha, India
S. Bahinipati[40], C. Kar, D. Maity[41], P. Mal, K. Naskar[41], A. Nayak[41], S. Nayak, K. Pal, P. Sadangi, S.K. Swain, S. Varghese[41], D. Vats[41]

Indian Institute of Science Education and Research (IISER), Pune, India
S. Acharya[42], A. Alpana, S. Dube, B. Gomber[42], P. Hazarika, B. Kansal, A. Laha, B. Sahu[42], S. Sharma, K.Y. Vaish

Isfahan University of Technology, Isfahan, Iran
H. Bakhshiansohi[43], A. Jafari[44], M. Zeinali[45]

Institute for Research in Fundamental Sciences (IPM), Tehran, Iran
S. Bashiri, S. Chenarani[46], S.M. Etesami, Y. Hosseini, M. Khakzad, E. Khazaie, M. Mohammadi Najafabadi, S. Tizchang[47]

University College Dublin, Dublin, Ireland
M. Felcini, M. Grunewald

INFN Sezione di Bari[a], Università di Bari[b], Politecnico di Bari[c], Bari, Italy
M. Abbrescia[a,b], A. Colaleo[a,b], D. Creanza[a,c], B. D'Anzi[a,b], N. De Filippis[a,c], M. De Palma[a,b], W. Elmetenawee[a,b,16], N. Ferrara[a,b], L. Fiore[a], G. Iaselli[a,c], L. Longo[a], M. Louka[a,b], G. Maggi[a,c], M. Maggi[a], I. Margjeka[a], V. Mastrapasqua[a,b], S. My[a,b], S. Nuzzo[a,b], A. Pellecchia[a,b], A. Pompili[a,b], G. Pugliese[a,c], R. Radogna[a,b], D. Ramos[a], A. Ranieri[a], L. Silvestris[a], F.M. Simone[a,c], Ü. Sözbilir[a], A. Stamerra[a,b], D. Troiano[a,b], R. Venditti[a,b], P. Verwilligen[a], A. Zaza[a,b]

INFN Sezione di Bologna[a], Università di Bologna[b], Bologna, Italy
G. Abbiendi[a], C. Battilana[a,b], D. Bonacorsi[a,b], P. Capiluppi[a,b], A. Castro[†a,b], F.R. Cavallo[a], M. Cuffiani[a,b], G.M. Dallavalle[a], T. Diotalevi[a,b], F. Fabbri[a], A. Fanfani[a,b], D. Fasanella[a], P. Giacomelli[a], L. Giommi[a,b], C. Grandi[a], L. Guiducci[a,b], S. Lo Meo[a,48], M. Lorusso[a,b], L. Lunerti[a], S. Marcellini[a], G. Masetti[a], F.L. Navarria[a,b], G. Paggi[a,b], A. Perrotta[a], F. Primavera[a,b], A.M. Rossi[a,b], S. Rossi Tisbeni[a,b], T. Rovelli[a,b], G.P. Siroli[a,b]

INFN Sezione di Catania[a], Università di Catania[b], Catania, Italy
S. Costa[a,b,49], A. Di Mattia[a], A. Lapertosa[a], R. Potenza[a,b], A. Tricomi[a,b,49]

INFN Sezione di Firenze[a], Università di Firenze[b], Firenze, Italy
P. Assiouras[a], G. Barbagli[a], G. Bardelli[a,b], B. Camaiani[a,b], A. Cassese[a], R. Ceccarelli[a], V. Ciulli[a,b], C. Civinini[a], R. D'Alessandro[a,b], E. Focardi[a,b], T. Kello[a], G. Latino[a,b], P. Lenzi[a,b], M. Lizzo[a], M. Meschini[a], S. Paoletti[a], A. Papanastassiou[a,b], G. Sguazzoni[a], L. Viliani[a]

INFN Laboratori Nazionali di Frascati, Frascati, Italy
L. Benussi, S. Bianco, S. Meola[50], D. Piccolo

INFN Sezione di Genova[a], Università di Genova[b], Genova, Italy
M. Alves Gallo Pereira[a], F. Ferro[a], E. Robutti[a], S. Tosi[a,b]

INFN Sezione di Milano-Bicocca[a], Università di Milano-Bicocca[b], Milano, Italy
A. Benaglia[a], F. Brivio[a], F. Cetorelli[a,b], F. De Guio[a,b], M.E. Dinardo[a,b], P. Dini[a], S. Gennai[a], R. Gerosa[a,b], A. Ghezzi[a,b], P. Govoni[a,b], L. Guzzi[a], M.T. Lucchini[a,b], M. Malberti[a], S. Malvezzi[a], A. Massironi[a], D. Menasce[a], L. Moroni[a], M. Paganoni[a,b], S. Palluotto[a,b], D. Pedrini[a], A. Perego[a,b], B.S. Pinolini[a], G. Pizzati[a,b], S. Ragazzi[a,b], T. Tabarelli de Fatis[a,b]

INFN Sezione di Napoli[a], Università di Napoli 'Federico II'[b], Napoli, Italy; Università della Basilicata[c], Potenza, Italy; Scuola Superiore Meridionale (SSM)[d], Napoli, Italy
S. Buontempo[a], A. Cagnotta[a,b], F. Carnevali[a,b], N. Cavallo[a,c], F. Fabozzi[a,c], A.O.M. Iorio[a,b], L. Lista[a,b,51], P. Paolucci[a,30], B. Rossi[a]

INFN Sezione di Padova[a], Università di Padova[b], Padova, Italy; Università di Trento[c], Trento, Italy
R. Ardino[a], P. Azzi[a], N. Bacchetta[a,52], D. Bisello[a,b], P. Bortignon[a], G. Bortolato[a,b], A. Bragagnolo[a,b], A.C.M. Bulla[a], R. Carlin[a,b], P. Checchia[a], T. Dorigo[a,53], F. Gasparini[a,b], U. Gasparini[a,b], S. Giorgetti[a], E. Lusiani[a], M. Margoni[a,b], M. Michelotto[a], M. Migliorini[a,b], J. Pazzini[a,b], P. Ronchese[a,b], R. Rossin[a,b], F. Simonetto[a,b], M. Tosi[a,b], A. Triossi[a,b], S. Ventura[a], M. Zanetti[a,b], P. Zotto[a,b], A. Zucchetta[a,b], G. Zumerle[a,b]

INFN Sezione di Pavia[a], Università di Pavia[b], Pavia, Italy
A. Braghieri[a], S. Calzaferri[a], D. Fiorina[a], P. Montagna[a,b], V. Re[a], C. Riccardi[a,b], P. Salvini[a], I. Vai[a,b], P. Vitulo[a,b]

INFN Sezione di Perugia[a], Università di Perugia[b], Perugia, Italy
S. Ajmal[a,b], M.E. Ascioti[a,b], G.M. Bilei[a], C. Carrivale[a,b], D. Ciangottini[a,b], L. Fanò[a,b], V. Mariani[a,b], M. Menichelli[a], F. Moscatelli[a,54], A. Rossi[a,b], A. Santocchia[a,b], D. Spiga[a], T. Tedeschi[a,b]

INFN Sezione di Pisa[a], Università di Pisa[b], Scuola Normale Superiore di Pisa[c], Pisa, Italy; Università di Siena[d], Siena, Italy
C. Aimè[a], C.A. Alexe[a,c], P. Asenov[a,b], P. Azzurri[a], G. Bagliesi[a], R. Bhattacharya[a], L. Bianchini[a,b], T. Boccali[a], E. Bossini[a], D. Bruschini[a,c], R. Castaldi[a], M.A. Ciocci[a,b], M. Cipriani[a,b], V. D'Amante[a,d], R. Dell'Orso[a], S. Donato[a], A. Giassi[a], F. Ligabue[a,c], A.C. Marini[a], D. Matos Figueiredo[a], A. Messineo[a,b], S. Mishra[a], V.K. Muraleedharan Nair Bindhu[a,b,41], M. Musich[a,b], S. Nandan[a], F. Palla[a], A. Rizzi[a,b], G. Rolandi[a,c], S. Roy Chowdhury[a], T. Sarkar[a], A. Scribano[a], P. Spagnolo[a], R. Tenchini[a], G. Tonelli[a,b], N. Turini[a,d], F. Vaselli[a,c], A. Venturi[a], P.G. Verdini[a]

INFN Sezione di Roma[a], Sapienza Università di Roma[b], Roma, Italy
P. Barria[a], C. Basile[a,b], F. Cavallari[a], L. Cunqueiro Mendez[a,b], D. Del Re[a,b], E. Di Marco[a,b], M. Diemoz[a], F. Errico[a,b], R. Gargiulo[a,b], E. Longo[a,b], L. Martikainen[a,b], J. Mijuskovic[a,b], G. Organtini[a,b], F. Pandolfi[a], R. Paramatti[a,b], C. Quaranta[a,b], S. Rahatlou[a,b], C. Rovelli[a], F. Santanastasio[a,b], L. Soffi[a], V. Vladimirov[a,b]

INFN Sezione di Torino[a], Università di Torino[b], Torino, Italy; Università del Piemonte Orientale[c], Novara, Italy
N. Amapane[a,b], R. Arcidiacono[a,c], S. Argiro[a,b], M. Arneodo[a,c], N. Bartosik[a], R. Bellan[a,b], C. Biino[a], C. Borca[a,b], N. Cartiglia[a], M. Costa[a,b], R. Covarelli[a,b], N. Demaria[a], L. Finco[a], M. Grippo[a,b], B. Kiani[a,b], F. Legger[a], F. Luongo[a,b], C. Mariotti[a], L. Markovic[a,b], S. Maselli[a], A. Mecca[a,b], L. Menzio[a,b], P. Meridiani[a], E. Migliore[a,b], M. Monteno[a], R. Mulargia[a], M.M. Obertino[a,b], G. Ortona[a], L. Pacher[a,b], N. Pastrone[a], M. Pelliccioni[a], M. Ruspa[a,c], F. Siviero[a,b], V. Sola[a,b], A. Solano[a,b], A. Staiano[a], C. Tarricone[a,b], D. Trocino[a], G. Umoret[a,b], R. White[a,b]

INFN Sezione di Trieste[a], Università di Trieste[b], Trieste, Italy
J. Babbar[a,b], S. Belforte[a], V. Candelise[a,b], M. Casarsa[a], F. Cossutti[a], K. De Leo[a], G. Della Ricca[a,b]

Kyungpook National University, Daegu, Korea
S. Dogra, J. Hong, J. Kim, D. Lee, H. Lee, S.W. Lee, C.S. Moon, Y.D. Oh, M.S. Ryu, S. Sekmen, B. Tae, Y.C. Yang

Department of Mathematics and Physics - GWNU, Gangneung, Korea
M.S. Kim

Chonnam National University, Institute for Universe and Elementary Particles, Kwangju, Korea
G. Bak, P. Gwak, H. Kim, D.H. Moon

Hanyang University, Seoul, Korea
E. Asilar, J. Choi[55], D. Kim, T.J. Kim, J.A. Merlin, Y. Ryou

Korea University, Seoul, Korea
S. Choi, S. Han, B. Hong, K. Lee, K.S. Lee, S. Lee, J. Yoo

Kyung Hee University, Department of Physics, Seoul, Korea
J. Goh, S. Yang

Sejong University, Seoul, Korea
H. S. Kim, Y. Kim, S. Lee

Seoul National University, Seoul, Korea
J. Almond, J.H. Bhyun, J. Choi, J. Choi, W. Jun, J. Kim, Y.W. Kim, S. Ko, H. Lee, J. Lee, J. Lee, B.H. Oh, S.B. Oh, H. Seo, U.K. Yang, I. Yoon

University of Seoul, Seoul, Korea
W. Jang, D.Y. Kang, Y. Kang, S. Kim, B. Ko, J.S.H. Lee, Y. Lee, I.C. Park, Y. Roh, I.J. Watson

Yonsei University, Department of Physics, Seoul, Korea
S. Ha, K. Hwang, B. Kim, H.D. Yoo

Sungkyunkwan University, Suwon, Korea
M. Choi, M.R. Kim, H. Lee, Y. Lee, I. Yu

College of Engineering and Technology, American University of the Middle East (AUM), Dasman, Kuwait
T. Beyrouthy, Y. Gharbia

Kuwait University - College of Science - Department of Physics, Safat, Kuwait

F. Alazemi

Riga Technical University, Riga, Latvia
K. Dreimanis, A. Gaile, C. Munoz Diaz, D. Osite, G. Pikurs, A. Potrebko, M. Seidel, D. Sidiropoulos Kontos

University of Latvia (LU), Riga, Latvia
N.R. Strautnieks

Vilnius University, Vilnius, Lithuania
M. Ambrozas, A. Juodagalvis, A. Rinkevicius, G. Tamulaitis

National Centre for Particle Physics, Universiti Malaya, Kuala Lumpur, Malaysia
I. Yusuff[56], Z. Zolkapli

Universidad de Sonora (UNISON), Hermosillo, Mexico
J.F. Benitez, A. Castaneda Hernandez, H.A. Encinas Acosta, L.G. Gallegos Maríñez, M. León Coello, J.A. Murillo Quijada, A. Sehrawat, L. Valencia Palomo

Centro de Investigacion y de Estudios Avanzados del IPN, Mexico City, Mexico
G. Ayala, H. Castilla-Valdez, H. Crotte Ledesma, E. De La Cruz-Burelo, I. Heredia-De La Cruz[57], R. Lopez-Fernandez, J. Mejia Guisao, C.A. Mondragon Herrera, A. Sánchez Hernández

Universidad Iberoamericana, Mexico City, Mexico
C. Oropeza Barrera, D.L. Ramirez Guadarrama, M. Ramírez García

Benemerita Universidad Autonoma de Puebla, Puebla, Mexico
I. Bautista, F.E. Neri Huerta, I. Pedraza, H.A. Salazar Ibarguen, C. Uribe Estrada

University of Montenegro, Podgorica, Montenegro
I. Bubanja, N. Raicevic

University of Canterbury, Christchurch, New Zealand
P.H. Butler

National Centre for Physics, Quaid-I-Azam University, Islamabad, Pakistan
A. Ahmad, M.I. Asghar, A. Awais, M.I.M. Awan, H.R. Hoorani, W.A. Khan

AGH University of Krakow, Krakow, Poland
V. Avati, A. Bellora, L. Forthomme, L. Grzanka, M. Malawski, K. Piotrzkowski

National Centre for Nuclear Research, Swierk, Poland
H. Bialkowska, M. Bluj, M. Górski, M. Kazana, M. Szleper, P. Zalewski

Institute of Experimental Physics, Faculty of Physics, University of Warsaw, Warsaw, Poland
K. Bunkowski, K. Doroba, A. Kalinowski, M. Konecki, J. Krolikowski, A. Muhammad

Warsaw University of Technology, Warsaw, Poland
P. Fokow, K. Pozniak, W. Zabolotny

Laboratório de Instrumentação e Física Experimental de Partículas, Lisboa, Portugal
M. Araujo, D. Bastos, C. Beirão Da Cruz E Silva, A. Boletti, M. Bozzo, T. Camporesi, G. Da Molin, P. Faccioli, M. Gallinaro, J. Hollar, N. Leonardo, G.B. Marozzo, A. Petrilli, M. Pisano, J. Seixas, J. Varela, J.W. Wulff

Faculty of Physics, University of Belgrade, Belgrade, Serbia

P. Adzic, P. Milenovic

VINCA Institute of Nuclear Sciences, University of Belgrade, Belgrade, Serbia
D. Devetak, M. Dordevic, J. Milosevic, L. Nadderd, V. Rekovic, M. Stojanovic

Centro de Investigaciones Energéticas Medioambientales y Tecnológicas (CIEMAT), Madrid, Spain
J. Alcaraz Maestre, Cristina F. Bedoya, J.A. Brochero Cifuentes, Oliver M. Carretero, M. Cepeda, M. Cerrada, N. Colino, B. De La Cruz, A. Delgado Peris, A. Escalante Del Valle, D. Fernández Del Val, J.P. Fernández Ramos, J. Flix, M.C. Fouz, O. Gonzalez Lopez, S. Goy Lopez, J.M. Hernandez, M.I. Josa, J. Llorente Merino, C. Martin Perez, E. Martin Viscasillas, D. Moran, C. M. Morcillo Perez, Á. Navarro Tobar, C. Perez Dengra, A. Pérez-Calero Yzquierdo, J. Puerta Pelayo, I. Redondo, J. Sastre, J. Vazquez Escobar

Universidad Autónoma de Madrid, Madrid, Spain
J.F. de Trocóniz

Universidad de Oviedo, Instituto Universitario de Ciencias y Tecnologías Espaciales de Asturias (ICTEA), Oviedo, Spain
B. Alvarez Gonzalez, J. Cuevas, J. Fernandez Menendez, S. Folgueras, I. Gonzalez Caballero, P. Leguina, E. Palencia Cortezon, J. Prado Pico, V. Rodríguez Bouza, A. Soto Rodríguez, A. Trapote, C. Vico Villalba, P. Vischia

Instituto de Física de Cantabria (IFCA), CSIC-Universidad de Cantabria, Santander, Spain
S. Blanco Fernández, I.J. Cabrillo, A. Calderon, J. Duarte Campderros, M. Fernandez, G. Gomez, C. Lasaosa García, R. Lopez Ruiz, C. Martinez Rivero, P. Martinez Ruiz del Arbol, F. Matorras, P. Matorras Cuevas, E. Navarrete Ramos, J. Piedra Gomez, L. Scodellaro, I. Vila, J.M. Vizan Garcia

University of Colombo, Colombo, Sri Lanka
B. Kailasapathy[58], D.D.C. Wickramarathna

University of Ruhuna, Department of Physics, Matara, Sri Lanka
W.G.D. Dharmaratna[59], K. Liyanage, N. Perera

CERN, European Organization for Nuclear Research, Geneva, Switzerland
D. Abbaneo, C. Amendola, E. Auffray, G. Auzinger, J. Baechler, D. Barney, A. Bermúdez Martínez, M. Bianco, A.A. Bin Anuar, A. Bocci, L. Borgonovi, C. Botta, E. Brondolin, C.E. Brown, C. Caillol, G. Cerminara, N. Chernyavskaya, D. d'Enterria, A. Dabrowski, A. David, A. De Roeck, M.M. Defranchis, M. Deile, M. Dobson, G. Franzoni, W. Funk, S. Giani, D. Gigi, K. Gill, F. Glege, J. Hegeman, J.K. Heikkilä, B. Huber, V. Innocente, T. James, P. Janot, O. Kaluzinska, O. Karacheban[28], G. Karathanasis, S. Laurila, P. Lecoq, E. Leutgeb, C. Lourenço, M. Magherini, L. Malgeri, M. Mannelli, M. Matthewman, A. Mehta, F. Meijers, S. Mersi, E. Meschi, V. Milosevic, F. Monti, F. Moortgat, M. Mulders, I. Neutelings, S. Orfanelli, F. Pantaleo, G. Petrucciani, A. Pfeiffer, M. Pierini, H. Qu, D. Rabady, B. Ribeiro Lopes, F. Riti, M. Rovere, H. Sakulin, R. Salvatico, S. Sanchez Cruz, S. Scarfi, C. Schwick, M. Selvaggi, A. Sharma, K. Shchelina, P. Silva, P. Sphicas[60], A.G. Stahl Leiton, A. Steen, S. Summers, D. Treille, P. Tropea, D. Walter, J. Wanczyk[61], J. Wang, S. Wuchterl, P. Zehetner, P. Zejdl, W.D. Zeuner

PSI Center for Neutron and Muon Sciences, Villigen, Switzerland

T. Bevilacqua[62], L. Caminada[62], A. Ebrahimi, W. Erdmann, R. Horisberger, Q. Ingram, H.C. Kaestli, D. Kotlinski, C. Lange, M. Missiroli[62], L. Noehte[62], T. Rohe, A. Samalan

ETH Zurich - Institute for Particle Physics and Astrophysics (IPA), Zurich, Switzerland
T.K. Aarrestad, M. Backhaus, G. Bonomelli, A. Calandri, C. Cazzaniga, K. Datta, P. De Bryas Dexmiers D'archiac[61], A. De Cosa, G. Dissertori, M. Dittmar, M. Donegà, F. Eble, M. Galli, K. Gedia, F. Glessgen, C. Grab, N. Härringer, T.G. Harte, D. Hits, W. Lustermann, A.-M. Lyon, R.A. Manzoni, M. Marchegiani, L. Marchese, A. Mascellani[61], F. Nessi-Tedaldi, F. Pauss, V. Perovic, S. Pigazzini, B. Ristic, R. Seidita, J. Steggemann[61], A. Tarabini, D. Valsecchi, R. Wallny

Universität Zürich, Zurich, Switzerland
C. Amsler[63], P. Bärtschi, M.F. Canelli, K. Cormier, M. Huwiler, W. Jin, A. Jofrehei, B. Kilminster, S. Leontsinis, S.P. Liechti, A. Macchiolo, P. Meiring, F. Meng, J. Motta, A. Reimers, P. Robmann, M. Senger, E. Shokr, F. Stäger, R. Tramontano

National Central University, Chung-Li, Taiwan
C. Adloff[64], D. Bhowmik, C.M. Kuo, W. Lin, P.K. Rout, P.C. Tiwari[38]

National Taiwan University (NTU), Taipei, Taiwan
L. Ceard, K.F. Chen, Z.g. Chen, A. De Iorio, W.-S. Hou, T.h. Hsu, Y.w. Kao, S. Karmakar, G. Kole, Y.y. Li, R.-S. Lu, E. Paganis, X.f. Su, J. Thomas-Wilsker, L.s. Tsai, D. Tsionou, H.y. Wu, E. Yazgan

High Energy Physics Research Unit, Department of Physics, Faculty of Science, Chulalongkorn University, Bangkok, Thailand
C. Asawatangtrakuldee, N. Srimanobhas, V. Wachirapusitanand

Tunis El Manar University, Tunis, Tunisia
Y. Maghrbi

Çukurova University, Physics Department, Science and Art Faculty, Adana, Turkey
D. Agyel, F. Boran, F. Dolek, I. Dumanoglu[65], E. Eskut, Y. Guler[66], E. Gurpinar Guler[66], C. Isik, O. Kara, A. Kayis Topaksu, Y. Komurcu, G. Onengut, K. Ozdemir[67], A. Polatoz, B. Tali[68], U.G. Tok, E. Uslan, I.S. Zorbakir

Middle East Technical University, Physics Department, Ankara, Turkey
M. Yalvac[69]

Bogazici University, Istanbul, Turkey
B. Akgun, I.O. Atakisi, E. Gülmez, M. Kaya[70], O. Kaya[71], S. Tekten[72]

Istanbul Technical University, Istanbul, Turkey
A. Cakir, K. Cankocak[65,73], S. Sen[74]

Istanbul University, Istanbul, Turkey
O. Aydilek[75], B. Hacisahinoglu, I. Hos[76], B. Kaynak, S. Ozkorucuklu, O. Potok, H. Sert, C. Simsek, C. Zorbilmez

Yildiz Technical University, Istanbul, Turkey
S. Cerci, B. Isildak[77], D. Sunar Cerci, T. Yetkin

Institute for Scintillation Materials of National Academy of Science of Ukraine, Kharkiv, Ukraine

A. Boyaryntsev, B. Grynyov

National Science Centre, Kharkiv Institute of Physics and Technology, Kharkiv, Ukraine
L. Levchuk

University of Bristol, Bristol, United Kingdom
D. Anthony, J.J. Brooke, A. Bundock, F. Bury, E. Clement, D. Cussans, H. Flacher, M. Glowacki, J. Goldstein, H.F. Heath, M.-L. Holmberg, L. Kreczko, S. Paramesvaran, L. Robertshaw, V.J. Smith, K. Walkingshaw Pass

Rutherford Appleton Laboratory, Didcot, United Kingdom
A.H. Ball, K.W. Bell, A. Belyaev[78], C. Brew, R.M. Brown, D.J.A. Cockerill, C. Cooke, A. Elliot, K.V. Ellis, K. Harder, S. Harper, J. Linacre, K. Manolopoulos, D.M. Newbold, E. Olaiya, D. Petyt, T. Reis, A.R. Sahasransu, G. Salvi, T. Schuh, C.H. Shepherd-Themistocleous, I.R. Tomalin, K.C. Whalen, T. Williams

Imperial College, London, United Kingdom
I. Andreou, R. Bainbridge, P. Bloch, O. Buchmuller, C.A. Carrillo Montoya, G.S. Chahal[79], D. Colling, J.S. Dancu, I. Das, P. Dauncey, G. Davies, M. Della Negra, S. Fayer, G. Fedi, G. Hall, A. Howard, G. Iles, C.R. Knight, P. Krueper, J. Langford, K.H. Law, J. León Holgado, L. Lyons, A.-M. Magnan, B. Maier, S. Mallios, M. Mieskolainen, J. Nash[80], M. Pesaresi, P.B. Pradeep, B.C. Radburn-Smith, A. Richards, A. Rose, K. Savva, C. Seez, R. Shukla, A. Tapper, K. Uchida, G.P. Uttley, T. Virdee[30], M. Vojinovic, N. Wardle, D. Winterbottom

Brunel University, Uxbridge, United Kingdom
J.E. Cole, A. Khan, P. Kyberd, I.D. Reid

Baylor University, Waco, Texas, USA
S. Abdullin, A. Brinkerhoff, E. Collins, M.R. Darwish, J. Dittmann, K. Hatakeyama, V. Hegde, J. Hiltbrand, B. McMaster, J. Samudio, S. Sawant, C. Sutantawibul, J. Wilson

Catholic University of America, Washington, DC, USA
R. Bartek, A. Dominguez, A.E. Simsek, S.S. Yu

The University of Alabama, Tuscaloosa, Alabama, USA
B. Bam, A. Buchot Perraguin, R. Chudasama, S.I. Cooper, C. Crovella, S.V. Gleyzer, E. Pearson, C.U. Perez, P. Rumerio[81], E. Usai, R. Yi

Boston University, Boston, Massachusetts, USA
A. Akpinar, C. Cosby, G. De Castro, Z. Demiragli, C. Erice, C. Fangmeier, C. Fernandez Madrazo, E. Fontanesi, D. Gastler, F. Golf, S. Jeon, J. O'cain, I. Reed, J. Rohlf, K. Salyer, D. Sperka, D. Spitzbart, I. Suarez, A. Tsatsos, A.G. Zecchinelli

Brown University, Providence, Rhode Island, USA
G. Barone, G. Benelli, D. Cutts, L. Gouskos, M. Hadley, U. Heintz, K.W. Ho, J.M. Hogan[82], T. Kwon, G. Landsberg, K.T. Lau, J. Luo, S. Mondal, T. Russell, S. Sagir[83], X. Shen, M. Stamenkovic, N. Venkatasubramanian

University of California, Davis, Davis, California, USA
S. Abbott, B. Barton, C. Brainerd, R. Breedon, H. Cai, M. Calderon De La Barca Sanchez, M. Chertok, M. Citron, J. Conway, P.T. Cox,

R. Erbacher, F. Jensen, O. Kukral, G. Mocellin, M. Mulhearn, S. Ostrom, W. Wei, S. Yoo, F. Zhang

University of California, Los Angeles, California, USA
K. Adamidis, M. Bachtis, D. Campos, R. Cousins, A. Datta, G. Flores Avila, J. Hauser, M. Ignatenko, M.A. Iqbal, T. Lam, Y.f. Lo, E. Manca, A. Nunez Del Prado, D. Saltzberg, V. Valuev

University of California, Riverside, Riverside, California, USA
R. Clare, J.W. Gary, G. Hanson

University of California, San Diego, La Jolla, California, USA
A. Aportela, A. Arora, J.G. Branson, S. Cittolin, S. Cooperstein, D. Diaz, J. Duarte, L. Giannini, Y. Gu, J. Guiang, R. Kansal, V. Krutelyov, R. Lee, J. Letts, M. Masciovecchio, F. Mokhtar, S. Mukherjee, M. Pieri, D. Primosch, M. Quinnan, V. Sharma, M. Tadel, E. Vourliotis, F. Würthwein, Y. Xiang, A. Yagil

University of California, Santa Barbara - Department of Physics, Santa Barbara, California, USA
A. Barzdukas, L. Brennan, C. Campagnari, K. Downham, C. Grieco, M.M. Hussain, J. Incandela, J. Kim, A.J. Li, P. Masterson, H. Mei, J. Richman, S.N. Santpur, U. Sarica, R. Schmitz, F. Setti, J. Sheplock, D. Stuart, T.Á. Vámi, X. Yan, D. Zhang

California Institute of Technology, Pasadena, California, USA
S. Bhattacharya, A. Bornheim, O. Cerri, J. Mao, H.B. Newman, G. Reales Gutiérrez, M. Spiropulu, J.R. Vlimant, C. Wang, S. Xie, R.Y. Zhu

Carnegie Mellon University, Pittsburgh, Pennsylvania, USA
J. Alison, S. An, P. Bryant, M. Cremonesi, V. Dutta, T. Ferguson, T.A. Gómez Espinosa, A. Harilal, A. Kallil Tharayil, C. Liu, T. Mudholkar, S. Murthy, P. Palit, K. Park, M. Paulini, A. Roberts, A. Sanchez, W. Terrill

University of Colorado Boulder, Boulder, Colorado, USA
J.P. Cumalat, W.T. Ford, A. Hart, A. Hassani, N. Manganelli, J. Pearkes, C. Savard, N. Schonbeck, K. Stenson, K.A. Ulmer, S.R. Wagner, N. Zipper, D. Zuolo

Cornell University, Ithaca, New York, USA
J. Alexander, X. Chen, D.J. Cranshaw, J. Dickinson, J. Fan, X. Fan, S. Hogan, P. Kotamnives, J. Monroy, M. Oshiro, J.R. Patterson, M. Reid, A. Ryd, J. Thom, P. Wittich, R. Zou

Fermi National Accelerator Laboratory, Batavia, Illinois, USA
M. Albrow, M. Alyari, O. Amram, G. Apollinari, A. Apresyan, L.A.T. Bauerdick, D. Berry, J. Berryhill, P.C. Bhat, K. Burkett, J.N. Butler, A. Canepa, G.B. Cerati, H.W.K. Cheung, F. Chlebana, G. Cummings, I. Dutta, V.D. Elvira, J. Freeman, A. Gandrakota, Z. Gecse, L. Gray, D. Green, A. Grummer, S. Grünendahl, D. Guerrero, O. Gutsche, R.M. Harris, T.C. Herwig, J. Hirschauer, B. Jayatilaka, S. Jindariani, M. Johnson, U. Joshi, T. Klijnsma, B. Klima, K.H.M. Kwok, S. Lammel, C. Lee, D. Lincoln, R. Lipton, T. Liu, K. Maeshima, D. Mason, P. McBride, P. Merkel, S. Mrenna, S. Nahn, J. Ngadiuba, D. Noonan, S. Norberg, V. Papadimitriou, N. Pastika, K. Pedro, C. Pena[84], F. Ravera,

A. Reinsvold Hall[85], L. Ristori, M. Safdari, E. Sexton-Kennedy, N. Smith, A. Soha, L. Spiegel, S. Stoynev, J. Strait, L. Taylor, S. Tkaczyk, N.V. Tran, L. Uplegger, E.W. Vaandering, I. Zoi

University of Florida, Gainesville, Florida, USA
C. Aruta, P. Avery, D. Bourilkov, P. Chang, V. Cherepanov, R.D. Field, C. Huh, E. Koenig, M. Kolosova, J. Konigsberg, A. Korytov, K. Matchev, N. Menendez, G. Mitselmakher, K. Mohrman, A. Muthirakalayil Madhu, N. Rawal, S. Rosenzweig, Y. Takahashi, J. Wang

Florida State University, Tallahassee, Florida, USA
T. Adams, A. Al Kadhim, A. Askew, S. Bower, R. Hashmi, R.S. Kim, S. Kim, T. Kolberg, G. Martinez, H. Prosper, P.R. Prova, M. Wulansatiti, R. Yohay, J. Zhang

Florida Institute of Technology, Melbourne, Florida, USA
B. Alsufyani, S. Butalla, S. Das, T. Elkafrawy[86], M. Hohlmann, E. Yanes

University of Illinois Chicago, Chicago, Illinois, USA
M.R. Adams, A. Baty, C. Bennett, R. Cavanaugh, R. Escobar Franco, O. Evdokimov, C.E. Gerber, M. Hawksworth, A. Hingrajiya, D.J. Hofman, J.h. Lee, D. S. Lemos, C. Mills, S. Nanda, G. Oh, B. Ozek, D. Pilipovic, R. Pradhan, E. Prifti, T. Roy, S. Rudrabhatla, N. Singh, M.B. Tonjes, N. Varelas, M.A. Wadud, Z. Ye, J. Yoo

The University of Iowa, Iowa City, Iowa, USA
M. Alhusseini, D. Blend, K. Dilsiz[87], L. Emediato, G. Karaman, O.K. Köseyan, J.-P. Merlo, A. Mestvirishvili[88], O. Neogi, H. Ogul[89], Y. Onel, A. Penzo, C. Snyder, E. Tiras[90]

Johns Hopkins University, Baltimore, Maryland, USA
B. Blumenfeld, L. Corcodilos, J. Davis, A.V. Gritsan, L. Kang, S. Kyriacou, P. Maksimovic, M. Roguljic, J. Roskes, S. Sekhar, M. Swartz

The University of Kansas, Lawrence, Kansas, USA
A. Abreu, L.F. Alcerro Alcerro, J. Anguiano, S. Arteaga Escatel, P. Baringer, A. Bean, Z. Flowers, D. Grove, J. King, G. Krintiras, M. Lazarovits, C. Le Mahieu, J. Marquez, M. Murray, M. Nickel, M. Pitt, S. Popescu[91], C. Rogan, C. Royon, S. Sanders, C. Smith, G. Wilson

Kansas State University, Manhattan, Kansas, USA
B. Allmond, R. Gujju Gurunadha, A. Ivanov, K. Kaadze, Y. Maravin, J. Natoli, D. Roy, G. Sorrentino

University of Maryland, College Park, Maryland, USA
A. Baden, A. Belloni, J. Bistany-riebman, Y.M. Chen, S.C. Eno, N.J. Hadley, S. Jabeen, R.G. Kellogg, T. Koeth, B. Kronheim, Y. Lai, S. Lascio, A.C. Mignerey, S. Nabili, C. Palmer, C. Papageorgakis, M.M. Paranjpe, E. Popova[92], A. Shevelev, L. Wang, L. Zhang

Massachusetts Institute of Technology, Cambridge, Massachusetts, USA
C. Baldenegro Barrera, J. Bendavid, S. Bright-Thonney, I.A. Cali, P.c. Chou, M. D'Alfonso, J. Eysermans, C. Freer, G. Gomez-Ceballos, M. Goncharov, G. Grosso, P. Harris, D. Hoang, D. Kovalskyi, J. Krupa, L. Lavezzo, Y.-J. Lee, K. Long, C. Mcginn, A. Novak, M.I. Park, C. Paus, C. Reissel, C. Roland, G. Roland,

S. Rothman, G.S.F. Stephans, Z. Wang, B. Wyslouch, T. J. Yang

University of Minnesota, Minneapolis, Minnesota, USA
B. Crossman, C. Kapsiak, M. Krohn, D. Mahon, J. Mans, B. Marzocchi, M. Revering, R. Rusack, R. Saradhy, N. Strobbe

University of Nebraska-Lincoln, Lincoln, Nebraska, USA
K. Bloom, D.R. Claes, G. Haza, J. Hossain, C. Joo, I. Kravchenko, A. Rohilla, J.E. Siado, W. Tabb, A. Vagnerini, A. Wightman, F. Yan, D. Yu

State University of New York at Buffalo, Buffalo, New York, USA
H. Bandyopadhyay, L. Hay, H.w. Hsia, I. Iashvili, A. Kalogeropoulos, A. Kharchilava, M. Morris, D. Nguyen, S. Rappoccio, H. Rejeb Sfar, A. Williams, P. Young

Northeastern University, Boston, Massachusetts, USA
G. Alverson, E. Barberis, J. Bonilla, B. Bylsma, M. Campana, J. Dervan, Y. Haddad, Y. Han, I. Israr, A. Krishna, P. Levchenko, J. Li, M. Lu, R. Mccarthy, D.M. Morse, V. Nguyen, T. Orimoto, A. Parker, L. Skinnari, E. Tsai, D. Wood

Northwestern University, Evanston, Illinois, USA
S. Dittmer, K.A. Hahn, D. Li, Y. Liu, M. Mcginnis, Y. Miao, D.G. Monk, M.H. Schmitt, A. Taliercio, M. Velasco

University of Notre Dame, Notre Dame, Indiana, USA
G. Agarwal, R. Band, R. Bucci, S. Castells, A. Das, R. Goldouzian, M. Hildreth, K. Hurtado Anampa, T. Ivanov, C. Jessop, K. Lannon, J. Lawrence, N. Loukas, L. Lutton, J. Mariano, N. Marinelli, I. Mcalister, T. McCauley, C. Mcgrady, C. Moore, Y. Musienko[23], H. Nelson, M. Osherson, A. Piccinelli, R. Ruchti, A. Townsend, Y. Wan, M. Wayne, H. Yockey, M. Zarucki, L. Zygala

The Ohio State University, Columbus, Ohio, USA
A. Basnet, M. Carrigan, L.S. Durkin, C. Hill, M. Joyce, M. Nunez Ornelas, K. Wei, D.A. Wenzl, B.L. Winer, B. R. Yates

Princeton University, Princeton, New Jersey, USA
H. Bouchamaoui, K. Coldham, P. Das, G. Dezoort, P. Elmer, A. Frankenthal, B. Greenberg, N. Haubrich, K. Kennedy, G. Kopp, S. Kwan, D. Lange, A. Loeliger, D. Marlow, I. Ojalvo, J. Olsen, F. Simpson, D. Stickland, C. Tully, L.H. Vage

University of Puerto Rico, Mayaguez, Puerto Rico, USA
S. Malik, R. Sharma

Purdue University, West Lafayette, Indiana, USA
A.S. Bakshi, S. Chandra, R. Chawla, A. Gu, L. Gutay, M. Jones, A.W. Jung, A.M. Koshy, M. Liu, G. Negro, N. Neumeister, G. Paspalaki, S. Piperov, V. Scheurer, J.F. Schulte, A. K. Virdi, F. Wang, A. Wildridge, W. Xie, Y. Yao

Purdue University Northwest, Hammond, Indiana, USA
J. Dolen, N. Parashar, A. Pathak

Rice University, Houston, Texas, USA
D. Acosta, A. Agrawal, T. Carnahan, K.M. Ecklund, P.J. Fernández Manteca,

S. Freed, P. Gardner, F.J.M. Geurts, I. Krommydas, W. Li, J. Lin, O. Miguel Colin, B.P. Padley, R. Redjimi, J. Rotter, E. Yigitbasi, Y. Zhang

University of Rochester, Rochester, New York, USA
A. Bodek, P. de Barbaro, R. Demina, J.L. Dulemba, A. Garcia-Bellido, O. Hindrichs, A. Khukhunaishvili, N. Parmar, P. Parygin[92], R. Taus

Rutgers, The State University of New Jersey, Piscataway, New Jersey, USA
B. Chiarito, J.P. Chou, S.V. Clark, D. Gadkari, Y. Gershtein, E. Halkiadakis, M. Heindl, C. Houghton, D. Jaroslawski, S. Konstantinou, I. Laflotte, A. Lath, R. Montalvo, K. Nash, J. Reichert, P. Saha, S. Salur, S. Schnetzer, S. Somalwar, R. Stone, S.A. Thayil, S. Thomas, J. Vora

University of Tennessee, Knoxville, Tennessee, USA
D. Ally, A.G. Delannoy, S. Fiorendi, S. Higginbotham, T. Holmes, A.R. Kanuganti, N. Karunarathna, L. Lee, E. Nibigira, S. Spanier

Texas A&M University, College Station, Texas, USA
D. Aebi, M. Ahmad, T. Akhter, K. Androsov[61], O. Bouhali[93], R. Eusebi, J. Gilmore, T. Huang, T. Kamon[94], H. Kim, S. Luo, R. Mueller, D. Overton, A. Safonov

Texas Tech University, Lubbock, Texas, USA
N. Akchurin, J. Damgov, Y. Feng, N. Gogate, Y. Kazhykarim, K. Lamichhane, S.W. Lee, C. Madrid, A. Mankel, T. Peltola, I. Volobouev

Vanderbilt University, Nashville, Tennessee, USA
E. Appelt, Y. Chen, S. Greene, A. Gurrola, W. Johns, R. Kunnawalkam Elayavalli, A. Melo, D. Rathjens, F. Romeo, P. Sheldon, S. Tuo, J. Velkovska, J. Viinikainen

University of Virginia, Charlottesville, Virginia, USA
B. Cardwell, H. Chung, B. Cox, J. Hakala, R. Hirosky, A. Ledovskoy, C. Mantilla, C. Neu, C. Ramón Álvarez

Wayne State University, Detroit, Michigan, USA
S. Bhattacharya, P.E. Karchin

University of Wisconsin - Madison, Madison, Wisconsin, USA
A. Aravind, S. Banerjee, K. Black, T. Bose, E. Chavez, S. Dasu, P. Everaerts, C. Galloni, H. He, M. Herndon, A. Herve, C.K. Koraka, A. Lanaro, R. Loveless, J. Madhusudanan Sreekala, A. Mallampalli, A. Mohammadi, S. Mondal, G. Parida, L. Pétré, D. Pinna, A. Savin, V. Shang, V. Sharma, W.H. Smith, D. Teague, H.F. Tsoi, W. Vetens, A. Warden

Authors affiliated with an international laboratory covered by a cooperation agreement with CERN
S. Afanasiev, V. Alexakhin, D. Budkouski, I. Golutvin[†], I. Gorbunov, V. Karjavine, O. Kodolova[95], V. Korenkov, A. Lanev, A. Malakhov, V. Matveev[96], A. Nikitenko[97,95], V. Palichik, V. Perelygin, M. Savina, V. Shalaev, S. Shmatov, S. Shulha, V. Smirnov, O. Teryaev, N. Voytishin, B.S. Yuldashev[†98], A. Zarubin, I. Zhizhin, Yu. Andreev, A. Dermenev, S. Gninenko, N. Golubev, A. Karneyeu, D. Kirpichnikov, M. Kirsanov, N. Krasnikov, I. Tlisova, A. Toropin

Authors affiliated with an institute formerly covered by a cooperation agreement with CERN
G. Gavrilov, V. Golovtcov, Y. Ivanov, V. Kim[99], V. Murzin, V. Oreshkin, D. Sos-

nov, V. Sulimov, L. Uvarov, A. Vorobyev†, T. Aushev, K. Ivanov, V. Gavrilov, N. Lychkovskaya, V. Popov, A. Zhokin, M. Chadeeva[99], R. Chistov[99], S. Polikarpov[99], V. Andreev, M. Azarkin, M. Kirakosyan, A. Terkulov, E. Boos, V. Bunichev, M. Dubinin[84], L. Dudko, A. Ershov, A. Gribushin, V. Klyukhin, S. Obraztsov, S. Petrushanko, V. Savrin, A. Snigirev, V. Blinov[99], T. Dimova[99], A. Kozyrev[99], O. Radchenko[99], Y. Skovpen[99], V. Kachanov, S. Slabospitskii, A. Uzunian, A. Babaev, V. Borshch, D. Druzhkin

†: Deceased
[1]Also at Yerevan State University, Yerevan, Armenia
[2]Also at TU Wien, Vienna, Austria
[3]Also at Ghent University, Ghent, Belgium
[4]Also at Universidade do Estado do Rio de Janeiro, Rio de Janeiro, Brazil
[5]Also at FACAMP - Faculdades de Campinas, Sao Paulo, Brazil
[6]Also at Universidade Estadual de Campinas, Campinas, Brazil
[7]Also at Federal University of Rio Grande do Sul, Porto Alegre, Brazil
[8]Also at University of Chinese Academy of Sciences, Beijing, China
[9]Also at China Center of Advanced Science and Technology, Beijing, China
[10]Also at University of Chinese Academy of Sciences, Beijing, China
[11]Also at China Spallation Neutron Source, Guangdong, China
[12]Now at Henan Normal University, Xinxiang, China
[13]Also at University of Shanghai for Science and Technology, Shanghai, China
[14]Now at The University of Iowa, Iowa City, Iowa, USA
[15]Also at an institute formerly covered by a cooperation agreement with CERN
[16]Also at Helwan University, Cairo, Egypt
[17]Now at Zewail City of Science and Technology, Zewail, Egypt
[18]Now at British University in Egypt, Cairo, Egypt
[19]Now at Cairo University, Cairo, Egypt
[20]Also at Purdue University, West Lafayette, Indiana, USA
[21]Also at Université de Haute Alsace, Mulhouse, France
[22]Also at Istinye University, Istanbul, Turkey
[23]Also at an international laboratory covered by a cooperation agreement with CERN
[24]Also at The University of the State of Amazonas, Manaus, Brazil
[25]Also at University of Hamburg, Hamburg, Germany
[26]Also at RWTH Aachen University, III. Physikalisches Institut A, Aachen, Germany
[27]Also at Bergische University Wuppertal (BUW), Wuppertal, Germany
[28]Also at Brandenburg University of Technology, Cottbus, Germany
[29]Also at Forschungszentrum Jülich, Juelich, Germany
[30]Also at CERN, European Organization for Nuclear Research, Geneva, Switzerland
[31]Also at HUN-REN ATOMKI - Institute of Nuclear Research, Debrecen, Hungary
[32]Now at Universitatea Babes-Bolyai - Facultatea de Fizica, Cluj-Napoca, Romania
[33]Also at MTA-ELTE Lendület CMS Particle and Nuclear Physics Group, Eötvös Loránd University, Budapest, Hungary
[34]Also at HUN-REN Wigner Research Centre for Physics, Budapest, Hungary
[35]Also at Physics Department, Faculty of Science, Assiut University, Assiut, Egypt
[36]Also at Punjab Agricultural University, Ludhiana, India
[37]Also at University of Visva-Bharati, Santiniketan, India
[38]Also at Indian Institute of Science (IISc), Bangalore, India
[39]Also at Amity University Uttar Pradesh, Noida, India
[40]Also at IIT Bhubaneswar, Bhubaneswar, India

[41]Also at Institute of Physics, Bhubaneswar, India
[42]Also at University of Hyderabad, Hyderabad, India
[43]Also at Deutsches Elektronen-Synchrotron, Hamburg, Germany
[44]Also at Isfahan University of Technology, Isfahan, Iran
[45]Also at Sharif University of Technology, Tehran, Iran
[46]Also at Department of Physics, University of Science and Technology of Mazandaran, Behshahr, Iran
[47]Also at Department of Physics, Faculty of Science, Arak University, ARAK, Iran
[48]Also at Italian National Agency for New Technologies, Energy and Sustainable Economic Development, Bologna, Italy
[49]Also at Centro Siciliano di Fisica Nucleare e di Struttura Della Materia, Catania, Italy
[50]Also at Università degli Studi Guglielmo Marconi, Roma, Italy
[51]Also at Scuola Superiore Meridionale, Università di Napoli 'Federico II', Napoli, Italy
[52]Also at Fermi National Accelerator Laboratory, Batavia, Illinois, USA
[53]Also at Lulea University of Technology, Lulea, Sweden
[54]Also at Consiglio Nazionale delle Ricerche - Istituto Officina dei Materiali, Perugia, Italy
[55]Also at Institut de Physique des 2 Infinis de Lyon (IP2I), Villeurbanne, France
[56]Also at Department of Applied Physics, Faculty of Science and Technology, Universiti Kebangsaan Malaysia, Bangi, Malaysia
[57]Also at Consejo Nacional de Ciencia y Tecnología, Mexico City, Mexico
[58]Also at Trincomalee Campus, Eastern University, Sri Lanka, Nilaveli, Sri Lanka
[59]Also at Saegis Campus, Nugegoda, Sri Lanka
[60]Also at National and Kapodistrian University of Athens, Athens, Greece
[61]Also at Ecole Polytechnique Fédérale Lausanne, Lausanne, Switzerland
[62]Also at Universität Zürich, Zurich, Switzerland
[63]Also at Stefan Meyer Institute for Subatomic Physics, Vienna, Austria
[64]Also at Laboratoire d'Annecy-le-Vieux de Physique des Particules, IN2P3-CNRS, Annecy-le-Vieux, France
[65]Also at Near East University, Research Center of Experimental Health Science, Mersin, Turkey
[66]Also at Konya Technical University, Konya, Turkey
[67]Also at Izmir Bakircay University, Izmir, Turkey
[68]Also at Adiyaman University, Adiyaman, Turkey
[69]Also at Bozok Universitetesi Rektörlügü, Yozgat, Turkey
[70]Also at Marmara University, Istanbul, Turkey
[71]Also at Milli Savunma University, Istanbul, Turkey
[72]Also at Kafkas University, Kars, Turkey
[73]Now at Istanbul Okan University, Istanbul, Turkey
[74]Also at Hacettepe University, Ankara, Turkey
[75]Also at Erzincan Binali Yildirim University, Erzincan, Turkey
[76]Also at Istanbul University - Cerrahpasa, Faculty of Engineering, Istanbul, Turkey
[77]Also at Yildiz Technical University, Istanbul, Turkey
[78]Also at School of Physics and Astronomy, University of Southampton, Southampton, United Kingdom
[79]Also at IPPP Durham University, Durham, United Kingdom
[80]Also at Monash University, Faculty of Science, Clayton, Australia
[81]Also at Università di Torino, Torino, Italy
[82]Also at Bethel University, St. Paul, Minnesota, USA
[83]Also at Karamanoğlu Mehmetbey University, Karaman, Turkey

[84]Also at California Institute of Technology, Pasadena, California, USA
[85]Also at United States Naval Academy, Annapolis, Maryland, USA
[86]Also at Ain Shams University, Cairo, Egypt
[87]Also at Bingol University, Bingol, Turkey
[88]Also at Georgian Technical University, Tbilisi, Georgia
[89]Also at Sinop University, Sinop, Turkey
[90]Also at Erciyes University, Kayseri, Turkey
[91]Also at Horia Hulubei National Institute of Physics and Nuclear Engineering (IFIN-HH), Bucharest, Romania
[92]Now at another institute formerly covered by a cooperation agreement with CERN
[93]Also at Texas A&M University at Qatar, Doha, Qatar
[94]Also at Kyungpook National University, Daegu, Korea
[95]Also at Yerevan Physics Institute, Yerevan, Armenia
[96]Also at another international laboratory covered by a cooperation agreement with CERN
[97]Also at Imperial College, London, United Kingdom
[98]Also at Institute of Nuclear Physics of the Uzbekistan Academy of Sciences, Tashkent, Uzbekistan
[99]Also at another institute formerly covered by a cooperation agreement with CERN